

# Universal quantum behaviors of interacting fermions in 1D traps: from few particles to the trap thermodynamic limit

Adriano Angelone, Massimo Campostrini and Ettore Vicari

*Dip. di Fisica dell'Università di Pisa and INFN, Largo Pontecorvo 3, I-56127 Pisa, Italy*

(Dated: August 16, 2021)

We investigate the ground-state properties of trapped fermion systems described by the Hubbard model with an external confining potential. We discuss the universal behaviors of systems in different regimes: from few particles, i.e. in dilute regime, to the trap thermodynamic limit.

The asymptotic trap-size (TS) dependence in the dilute regime (increasing the trap size  $\ell$  keeping the particle number  $N$  fixed) is described by a universal TS scaling controlled by the dilute fixed point associated with the metal-to-vacuum quantum transition. This scaling behavior is numerically checked by DMRG simulations of the one-dimensional (1D) Hubbard model. In particular, the particle density and its correlations show crossovers among different regimes: for strongly repulsive interactions they approach those of a spinless Fermi gas, for weak interactions those of a free Fermi gas, and for strongly attractive interactions they match those of a gas of hard-core bosonic molecules.

The large- $N$  limit keeping the ratio  $N/\ell$  fixed corresponds to a 1D trap thermodynamic limit. We address issues related to the accuracy of the local density approximation (LDA). We show that the particle density approaches its LDA in the large- $\ell$  limit. When the trapped system is in the metallic phase, corrections at finite  $\ell$  are  $O(\ell^{-1})$  and oscillating around the center of the trap. They become significantly larger at the boundary of the fermion cloud, where they get suppressed as  $O(\ell^{-1/3})$  only. This anomalous behavior arises from the nontrivial scaling at the metal-to-vacuum transition occurring at the boundaries of the fermion cloud.

PACS numbers: 71.10.Fd, 05.30.Fk, 67.85.-d, 05.10.Cc

## I. INTRODUCTION

The progress in the experimental activity in atomic physics, quantum optics and nanoscience has provided a great opportunity to investigate the nature of the quantum dynamics, and the interplay between quantum and statistical behaviors in particle systems. In particular, experiments with cold atoms realize systems which are accurately described by microscopic theoretical models such as dilute atomic Fermi and Bose gases, or Hubbard and Bose-Hubbard models in optical lattices. See e.g. Refs. [1–4]. A peculiar feature of these experiments is the confinement of the atoms, i.e. the presence of an inhomogeneous space-dependent (usually harmonic) trapping potential. The tunability of the confining potential allows the realization of quasi-two and quasi-one dimensional systems, by tightly confining the particles along one or two transverse dimensions.

The inhomogeneity induced by the trapping potential gives rise to peculiar effects, such as the possibility of simultaneously observing different phases, in particular Mott incompressible (insulator) and superfluid (metallic) phases, depending on the distance from the center of the trap. [1–3] This is essentially due to the fact that the effective local chemical potential decreases with increasing the distance from the center of the trap center. At continuous quantum transitions the presence of the trap does not allow the development of critical modes with diverging length scales. However, in the limit of large trap size  $\ell$  the system develops peculiar critical modes, which give rise to a universal trap-size scaling (TSS), controlled by the universality class of the transition of the

homogeneous system [5, 6]. Therefore, in experiments of trapped particle systems, a thorough understanding of the quantum many-body dynamics calls for a quantitative analysis of the trap effects. This issue has been much discussed by theoretical and experimental investigations, see e.g. Refs. 5–55.

In this paper we consider spin-1/2 fermion systems described by the lattice Hubbard model, at zero temperature, therefore in their ground state. We investigate the scaling behavior of unpolarized systems, i.e. with equal number of spin-down and spin-up particles, when varying the size of the trap confining the particles. We mostly consider one-dimensional (1D) systems with both attractive and repulsive interactions, in the dilute regime when the trap size  $\ell$  increases keeping the particle number  $N$  fixed, and in the *trap thermodynamic* limit defined as the large- $N$  limit keeping the ratio  $N/\ell$  fixed. Note that 1D fermion systems are also experimentally interesting, indeed their realizations, and evidences of pairing, have been recently reported in Refs. [56, 57].

The asymptotic trap-size dependence in the dilute regime for a system of  $N$  particles can be described in the framework of the TSS theory, whose scaling behavior is controlled by the dilute fixed point associated with the metal-to-vacuum quantum transition. This is controlled by the trap exponent  $\theta$  related to the renormalization-group (RG) perturbation arising from the trapping potential, and requires a nontrivial rescaling of the on-site interaction in 1D systems. The TSS predictions are compared with numerical results based on DMRG simulations. In particular, we address issues related to the expected crossover from strongly repulsive interactions,

where the system assumes the properties of a free spinless Fermi gas, to strongly attractive interactions, where the system is expected to be effectively constituted by hard-core bosonic (spin zero) molecules of two fermions, passing through a free Fermi gas in the absence of interactions.

We also investigate the trap thermodynamic limit of the Hubbard model, i.e. the large- $\ell$  and large- $N$  limit keeping the ratio  $N/\ell^d$  fixed. In particular, we address issues related to the accuracy of the local-density approximation (LDA), which approximates the space-dependent particle density of an inhomogeneous trap by the particle density of the homogeneous system at the corresponding value of the effective chemical potential. LDA is usually used to determine the particle density in inhomogeneous systems, providing an accurate approximation when the inhomogeneity is sufficiently smooth. Of course, LDA is not exact, in particular at finite trap sizes. Therefore, an analysis of the deviations from LDA, and therefore of its accuracy, is required to get a robust confidence of its results.

LDA has been largely employed in studies of inhomogeneous interacting fermion systems, see Refs. [1–4] and references therein, in particular of 1D systems [7, 9, 10, 13, 14, 16, 17, 19–27, 41–43, 48]. The comparison with numerical results for the particle density shows that it provides a good approximation in many cases. A more quantitative analysis of the deviations from LDA may be achieved by establishing whether LDA becomes exact in the large trap-size limit, and how deviations get suppressed at large, but finite,  $\ell$ . We investigate this issue in the trapped 1D Hubbard model, where LDA of the particle density can be exactly computed by Bethe-Ansatz methods [58, 59], allowing us to perform an accurate study of the deviations from LDA. We show that LDA of the particle density tends to become exact in the large trap-size limit, with power-law suppressed corrections. In particular, the corrections appear significantly larger at the boundary of the fermion cloud, decreasing as  $O(\ell^{-1/3})$ , due to the critical modes arising from the metal-to-vacuum transition at the edges of the trap.

The paper is organized as follows. In Sec. II we present the Hubbard model in the presence of an external potential coupled to the particle density; we provide the definitions of the observables and correlations which are considered in the paper. In Sec. III we investigate the trap-size dependence at a fixed particle number, i.e. in the dilute regime, in the framework of the TSS theory. In Sec. IV we consider the thermodynamic limit in a trap, i.e. the large trap-size limit keeping the ratio  $N/\ell$  fixed; in particular, we address the accuracy of the LDA of the particle density and the peculiar scaling behavior at the boundary of the cloud. Finally, in Sec. V we summarize our main results and draw our conclusions. Some appendices report technical details of some results mentioned in the paper.

## II. THE HUBBARD MODEL

The Hamiltonian of the Hubbard model reads

$$H = -t \sum_{\sigma, \langle \mathbf{x}\mathbf{y} \rangle} (c_{\sigma\mathbf{x}}^\dagger c_{\sigma\mathbf{y}} + \text{h.c.}) + U \sum_{\mathbf{x}} n_{\uparrow\mathbf{x}} n_{\downarrow\mathbf{x}} \quad (1)$$

where  $\mathbf{x}$  are the sites of a cubic lattice,  $\langle \mathbf{x}\mathbf{y} \rangle$  indicates nearest-neighbor sites,  $c_{\sigma\mathbf{x}}$  is a fermionic operator,  $\sigma = \uparrow\downarrow$  labels the spin states, and  $n_{\sigma\mathbf{x}} \equiv c_{\sigma\mathbf{x}}^\dagger c_{\sigma\mathbf{x}}$ . The particle number operators  $\hat{N}_\sigma = \sum_{\mathbf{x}} n_{\sigma\mathbf{x}}$  are conserved, i.e.  $[H, \hat{N}_\sigma] = 0$ . In the following we consider balanced Fermi systems, thus

$$N_\uparrow = N_\downarrow = N/2 \quad (2)$$

where  $N$  is the total number of particles. In this symmetric case  $\langle n_{\uparrow\mathbf{x}} \rangle = \langle n_{\downarrow\mathbf{x}} \rangle$  and  $\langle c_{\uparrow\mathbf{x}}^\dagger c_{\uparrow\mathbf{y}} \rangle = \langle c_{\downarrow\mathbf{x}}^\dagger c_{\downarrow\mathbf{y}} \rangle$ .

The presence of a trapping potential can be taken into account by adding an external-potential term in the Hamiltonian of the Hubbard model,

$$H_t = H + H_e, \quad (3)$$

$$H_e = \sum_{\mathbf{x}} V(\mathbf{x}) n_{\mathbf{x}}, \quad n_{\mathbf{x}} \equiv \sum_{\sigma} n_{\sigma\mathbf{x}}. \quad (4)$$

For simplicity, we assume a rotational invariant potential

$$V(\mathbf{x}) = \frac{1}{p} v^p r^p, \quad r \equiv |\mathbf{x}|, \quad (5)$$

where  $r$  is the distance from the center of the trap, and  $p$  is a positive number. We set the origin  $\mathbf{x} = 0$  at the center of the trap. The trap size  $\ell$  is defined as

$$\ell \equiv \frac{(2t)^{1/p}}{v}, \quad V(\mathbf{x}) = 2t \frac{r^p}{p\ell^p} \quad (6)$$

The trapping potential is effectively harmonic in most experiments, i.e.  $p = 2$ . [1] In the limit  $p \rightarrow \infty$  we recover a homogeneous spherical system of size  $L = 2\ell$  with hard-wall boundary conditions.

The above definition of trap size  $\ell$  naturally arises when we consider a thermodynamic limit in a trap [1, 60]. Indeed, in the presence of trap, a *trap thermodynamic* limit can be consistently defined as the large- $\ell$  limit keeping the ratio  $N/\ell^d$  fixed. This is equivalent to introducing a chemical potential  $\mu$ , by adding the term

$$H_\mu = -\mu \sum_{\mathbf{x}} n_{\mathbf{x}} \quad (7)$$

to the Hubbard Hamiltonian (1).

In the rest of the paper we set the kinetic constant  $t = 1$  and  $\hbar = 1$ ; their dependence can be easily inferred by dimensional analyses.

In our study we focus on the ground-state properties. We consider one-point observables such as the particle density

$$\rho(\mathbf{x}) = \langle n_{\mathbf{x}} \rangle \quad (8)$$

and the double occupancy

$$d_o(\mathbf{x}) = \langle n_{\uparrow\mathbf{x}}n_{\downarrow\mathbf{x}} \rangle. \quad (9)$$

Moreover, we analyze the behavior of correlation functions such as the one-particle correlation

$$C(\mathbf{x}, \mathbf{y}) = \sum_{\sigma} \langle c_{\sigma\mathbf{x}}^{\dagger} c_{\sigma\mathbf{y}} + \text{h.c.} \rangle, \quad (10)$$

the connected density-density correlations

$$G(\mathbf{x}, \mathbf{y}) = \langle n_{\mathbf{x}}n_{\mathbf{y}} \rangle - \langle n_{\mathbf{x}} \rangle \langle n_{\mathbf{y}} \rangle, \quad (11)$$

$$M(\mathbf{x}, \mathbf{y}) = \langle n_{\uparrow\mathbf{x}}n_{\downarrow\mathbf{y}} \rangle - \langle n_{\uparrow\mathbf{x}} \rangle \langle n_{\downarrow\mathbf{y}} \rangle, \quad (12)$$

and the pair correlation

$$P(\mathbf{x}, \mathbf{y}) = \langle c_{\uparrow\mathbf{x}}^{\dagger} c_{\downarrow\mathbf{x}}^{\dagger} c_{\downarrow\mathbf{y}} c_{\uparrow\mathbf{y}} + \text{h.c.} \rangle. \quad (13)$$

In the following we mostly consider 1D systems. The homogeneous 1D Hubbard model has been extensively studied, obtaining several exact results, see e.g. Ref. [59]. The phase diagram of homogenous 1D unpolarized systems presents various quantum phases related to the behavior of the particle density, such as vacuum, metallic and Mott insulator (incompressible) phases, depending on the chemical potential  $\mu$  and the on-site interaction  $U$ . Their phase boundaries are known exactly, by computations based on the Bethe Ansatz, see e.g. Ref. [59]. In particular, the vacuum-to-metal transition occurs at

$$\mu_0 = -2 \quad \text{for } U \geq 0, \quad (14)$$

$$\mu_0 = -2\sqrt{1 + \frac{U^2}{16}} \quad \text{for } U < 0. \quad (15)$$

Fig. 1 shows the phase diagram for the 1D unpolarized Hubbard model, with the different phases characterized by different behaviors of the particle density. In the metallic phase region the low-energy properties are characterized by algebraically decaying correlations [59, 61]. At small attractive interactions fermions form Cooper-pair-like bound states resembling those of BCS superconductors, while in the limit of strong interactions the pairs become tightly bounded within an extension of the lattice spacing, giving effectively rise to a system of hard-core bosons.

We finally mention that the 1D Hubbard model, even in the presence of an external confining potential, can be exactly mapped into a model of two interacting species (flavors) of hard-core bosons described by a Bose-Hubbard model, whose Hamiltonian is formally analogous to that of the Hubbard model with the fermionic operators  $c_{\sigma x}$  replaced by hard-core bosonic operators  $b_{\sigma x}$ . Some details are reported in App. A. The mapping between fermionic and bosonic operators is nonlocal, but it directly maps the density operator of fermions into that of bosons, i.e.  $c_{\sigma x}^{\dagger} c_{\sigma x} \rightarrow b_{\sigma x}^{\dagger} b_{\sigma x}$ . Thus the particle density and its correlations for the fermionic Hubbard model are identical to those of the two-flavor Bose-Hubbard model.

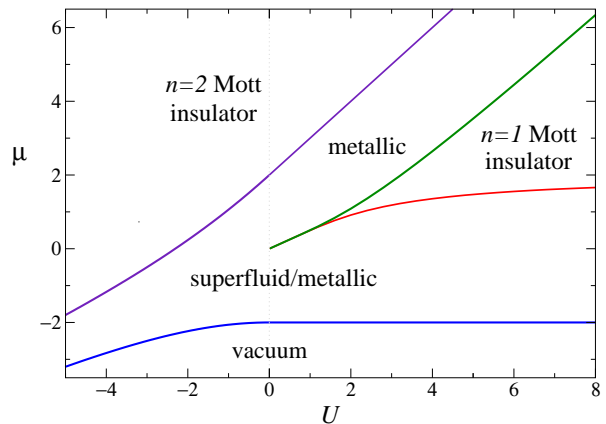


FIG. 1: (Color online) Phase diagram of the 1D unpolarized Hubbard model, which shows the different quantum phases related to the behavior of the particle density: vacuum, metal,  $n = 1$  and  $n = 2$  Mott insulator phases.

### III. TRAP-SIZE SCALING IN THE DILUTE REGIME

In this section we study the asymptotic trap-size dependence in the dilute regime, when increasing the trap size while keeping the particle number  $N$  fixed. This issue is best addressed in the framework of the TSS theory [6]. Its universal features are determined by the RG dimensions of the relevant perturbations at the fixed point controlling the vacuum-to-metal transition of the Hubbard model.

The scaling behavior of the Hubbard model in the dilute regime can be inferred by a RG analysis of the corresponding quantum field theory, see e.g. Ref. [62],

$$Z_F = \int D\psi_{\sigma}^* D\psi_{\sigma} \exp \left( - \int_0^{1/T} d\tau \int d^d x \mathcal{L}_F \right), \quad (16)$$

$$\mathcal{L}_F = \sum_{\sigma} \left[ \psi_{\sigma}^* \frac{\partial \psi_{\sigma}}{\partial \tau} + \frac{1}{2m} |\nabla \psi_{\sigma}|^2 - \mu |\psi_{\sigma}|^2 \right] + u \psi_{\uparrow}^* \psi_{\downarrow}^* \psi_{\downarrow} \psi_{\uparrow}.$$

The dynamic critical exponent  $z$  and the RG dimensions  $y_{\mu}$  and  $y_u$  of the relevant parameter  $\mu$  and  $u$  at the dilute fixed point ( $\mu = 0$  and  $u = 0$ ) encode most important information on the scaling properties in the dilute regime. Since the dilute fixed point is essentially Gaussian, they can be obtained by simple dimensional analyses,

$$z = 2, \quad y_{\mu} = 2, \quad y_u = 2 - d. \quad (17)$$

In order to obtain the scaling behavior of the observables, such as the particle density and the correlations introduced in Sec. II, we also need the RG dimensions of the fermionic field  $\psi$ , density operator  $n = \psi^{\dagger} \psi$ , and pair operator  $p = \psi_{\uparrow} \psi_{\downarrow}$ , which are respectively  $y_{\psi} = d/2$  and  $y_n = y_p = d$ .

The trap effects in the dilute regime can be inferred by analyzing the RG perturbation arising from an external

confining potential  $V(\mathbf{x})$  such as that of Eq. (5), i.e.

$$P_V(\mathbf{x}) = V(\mathbf{x}) \sum_{\sigma} |\psi_{\sigma}(\mathbf{x})|^2, \quad V(\mathbf{x}) = v^p |\mathbf{x}|^p, \quad (18)$$

at the dilute fixed point. Proceeding analogously to the case of spinless free-fermion systems [39, 40], the RG dimension  $y_v$  of the potential coupling  $v$  can be obtained from the RG relation

$$py_v - p = d + z - y_n = y_{\mu}. \quad (19)$$

This RG analysis tells us that the trap induces a length scale

$$\xi \sim \ell^{\theta} \quad (20)$$

with

$$\theta \equiv \frac{1}{y_v} = \frac{p}{p + y_{\mu}} = \frac{p}{p + 2}. \quad (21)$$

This implies that the spatial coordinates  $\mathbf{x}$  must be rescaled as  $\mathbf{X} = \mathbf{x}/\ell^{\theta}$  to get a nontrivial TSS limit. In particular,  $\theta = 1/2$  for the harmonic  $p = 2$  potential, in any spatial dimension.

The knowledge of the above critical exponents and RG dimensions allows us to write down the universal TSS ansatz for the observables introduced in Sec. II in the dilute regime, which provides the asymptotic behavior of their trap-size dependence. For example, for the  $n$ -point correlation of a generic local operator  $\mathcal{O}(\mathbf{x})$ , we expect [6, 39]

$$F(\mathbf{x}_1, \dots, \mathbf{x}_n; \ell, U, N) \equiv \langle \mathcal{O}(\mathbf{x}_1) \dots \mathcal{O}(\mathbf{x}_n) \rangle \quad (22)$$

$$\approx \ell^{-\varepsilon} \mathcal{F}(\mathbf{X}_1, \dots, \mathbf{X}_n; U \ell^{\theta y_{\mu}}, N)$$

where

$$\varepsilon = n\theta y_o, \quad \mathbf{X}_i = \mathbf{x}_i/\ell^{\theta}, \quad (23)$$

and  $y_o$  is the RG dimension of the operator  $\mathcal{O}(\mathbf{x})$  at the dilute fixed point. Corrections to the above asymptotic behavior are generally suppressed by further negative powers of  $\ell$ . TSS has some analogies with the standard FSS for homogeneous systems [63, 64] with two main differences: the inhomogeneity due to the space dependence of the external field, and the size  $L$  replaced by  $\ell^{\theta}$ .

### A. TSS in a lattice gas of free spinless fermions

The trap-size dependence of the simplest noninteracting case  $U = 0$  can be easily determined using the results obtained for trapped lattice gases of spinless fermions, defined by

$$H = - \sum_{\langle \mathbf{x}\mathbf{y} \rangle} (c_{\mathbf{x}}^{\dagger} c_{\mathbf{y}} + \text{h.c.}) + \sum_{\mathbf{x}} V(\mathbf{x}) n_{\mathbf{x}}, \quad (24)$$

where  $c_{\mathbf{x}}$  is a spinless fermionic operator,  $n_{\mathbf{x}} = c_{\mathbf{x}}^{\dagger} c_{\mathbf{x}}$ , and the potential  $V(\mathbf{x})$  is given in Eq. (5). In the following we report some of the results of Refs. [40, 65] which are useful for the rest of the paper.

In arbitrary dimensions the asymptotic trap-size dependence of the particle density of a free gas of  $N$  spinless fermions ( $N = \langle \hat{N} \rangle$  and  $\hat{N} = \sum_{\mathbf{x}} n_{\mathbf{x}}$ ) is given by [40]

$$\rho(\mathbf{x}, \ell, N) \approx \ell^{-d\theta} S_p(\mathbf{X}, N), \quad (25)$$

where  $\theta$  is the same trap exponent (21), and  $\mathbf{X} \equiv \mathbf{x}/\ell^{\theta}$ . As shown in Refs. [6, 40], the TSS limit corresponds to a continuum limit in the presence of the trap. Thus the TSS functions providing the asymptotic trap-size dependence can be exactly derived from the ground state of a trapped spinless Fermi gas defined in the continuum. This is given by a Slater determinant of the lowest  $N$  one-particle eigenfunctions  $\varphi_k(\mathbf{x})$  of the Schrödinger problem

$$H\varphi_k = \varepsilon_k \varphi_k, \quad H = \frac{1}{2} \mathbf{p}^2 + \frac{1}{p} |\mathbf{x}|^p, \quad (26)$$

with unit mass and trap size. This allows us to write the TSS function  $S_p$  in Eq. (25) as

$$S_p(\mathbf{X}, N) = \sum_{k=1}^N \varphi_k(\mathbf{X})^2. \quad (27)$$

In particular, in the case of 1D systems in a harmonic trap, it can be written as [10, 65]

$$S_2(x, N) = \frac{\sqrt{N}}{\sqrt{2}} [\varphi'_{N+1}(x) \varphi_N(x) - \varphi'_N(x) \varphi_{N+1}(x)] \quad (28)$$

where

$$\varphi_k(x) = \frac{H_{k-1}(x)}{\pi^{1/4} 2^{(k-1)/2} (k-1)!^{1/2}} e^{-x^2/2},$$

$H_k$  are the Hermite polynomials, and the corresponding eigenvalues are  $\varepsilon_k \propto k - 1/2$ . In the case of a 1D hard-wall trap, corresponding to  $p \rightarrow \infty$ ,

$$S_{\infty}(x, N) = \frac{N}{2} + \frac{1}{4} - \frac{\sin[\pi(N + 1/2)(1 + x)]}{4 \sin[\pi(1 + x)/2]} \quad (29)$$

with  $|x| \leq 1$ .

The one particle correlation behaves as

$$C(\mathbf{x}_1, \mathbf{x}_2, \ell, N) \approx \ell^{-d\theta} E_p(\mathbf{X}_1, \mathbf{X}_2, N), \quad (30)$$

where  $\mathbf{X}_i = \mathbf{x}_i/\ell^{\theta}$  and

$$E_p(\mathbf{X}_1, \mathbf{X}_2, N) = \sum_{k=1}^N \varphi_k(\mathbf{X}_1) \varphi_k(\mathbf{X}_2). \quad (31)$$

The connected density correlation scales asymptotically as

$$G(\mathbf{x}_1, \mathbf{x}_2, \ell, N) \approx \ell^{-2d\theta} Y_p(\mathbf{X}_1, \mathbf{X}_2, N), \quad (32)$$

$$Y_p(\mathbf{X}_1, \mathbf{X}_2, N) = -E_p(\mathbf{X}_1, \mathbf{X}_2, N)^2 \quad (33)$$

for  $|\mathbf{x}_1 - \mathbf{x}_2| > 0$ , which can be derived from the free fermion relation

$$G(\mathbf{x}_1, \mathbf{x}_2) = -|C(\mathbf{x}_1, \mathbf{x}_2)|^2 + \delta(\mathbf{x}_1 - \mathbf{x}_2)C(\mathbf{x}_1, \mathbf{x}_2). \quad (34)$$

Corrections to the above large- $\ell$  scaling behavior are  $O(\ell^{-2\theta})$  relatively to the leading term [6].

The above TSS behaviors are universal with respect to a large class of short-range interactions. For example, the same asymptotic behavior is also expected in the presence of a density-density nearest-neighbour interaction [39]

$$H_{nn} = w \sum_{\langle \mathbf{x}\mathbf{y} \rangle} n_{\mathbf{x}} n_{\mathbf{y}}. \quad (35)$$

Indeed the RG dimension of the coupling  $w$  is [62]  $y_w = -d$ , thus the interaction  $H_{nn}$  only induces  $O(\ell^{-d\theta})$  corrections to the asymptotic behaviors.

The TSS functions of the particle density and the one-particle and density correlations, cf. Eqs. (25), (30) and (32), show also peculiar large- $N$  scaling behaviors. Indeed, [65]

$$S_p(\mathbf{x}, N) \approx N^\theta \mathcal{S}_p(N^{(\theta-1)/d} \mathbf{X}), \quad (36)$$

and

$$E_p(\mathbf{X}_1, \mathbf{X}_2, N) \approx N^\theta \mathcal{E}_p(N^{\theta/d} \mathbf{X}_1, N^{\theta/d} \mathbf{X}_2), \quad (37)$$

$$Y_p(\mathbf{X}_1, \mathbf{X}_2, N) \approx N^{2\theta} \mathcal{Y}_p(N^{\theta/d} \mathbf{X}_1, N^{\theta/d} \mathbf{X}_2). \quad (38)$$

Note the different scaling of the space variable between the density and the one-particle and connected density correlations.

In the case of 1D systems in a harmonic trap, the large- $N$  scaling behavior can be derived from Eq. (28), obtaining

$$S_2(X, N) \approx N^{1/2} \mathcal{S}_2(X/N^{1/2}), \quad (39)$$

$$S_2(z) = \frac{1}{\pi} \sqrt{2 - z^2} \quad \text{for } z \leq z_b = \sqrt{2}, \quad (40)$$

and  $S_2(z) = 0$  for  $z \geq z_b$ . The corrections to this large- $N$  behavior are known [40]; they are  $O(N^{-1})$  (relatively to the leading term) for  $z < z_b$ . In particular,

$$S_2(0, N) = \frac{\sqrt{2}}{\pi} N^{1/2} \left[ 1 + \frac{(-1)^{N+1}}{4N} + \dots \right] \quad (41)$$

We finally mention that around the boundary of the trap, i.e. at the spatial point  $z = \pm z_b = \sqrt{2}$  where the function  $S_2$  vanishes, a different large- $N$  scaling behavior sets in: [40, 66]

$$\begin{aligned} \lim_{N \rightarrow \infty} N^{-1/6} S_2(N^{1/2} z_b + N^{-1/6} z, N) &= F(z), \\ F(z) &= 2^{1/2} |\text{Ai}'(2^{1/2} z)|^2 - 2z |\text{Ai}(2^{1/2} z)|^2. \end{aligned} \quad (42)$$

This implies that at the boundary  $z_b$  of the cloud the TSS function of the particle density increases as  $N^{1/6}$  only, instead of the  $O(N^{1/2})$  behavior for  $|z| < z_b$ . This is related to the fact that the  $z \rightarrow z_b$  limit of the  $O(1/N)$  corrections is singular, see also below.

In the following we extend these results to the Hubbard model, and in general to lattice fermion gases with short-range interactions.

## B. TSS in the dilute regime of the Hubbard model

### 1. TSS for $d > 2$

The RG analysis leading to Eqs. (17) shows that the  $U$  term is irrelevant at the dilute fixed point for  $d > 2$ , because its RG dimension  $y_u$  is negative. Therefore, the asymptotic trap-size dependence in the dilute regime turns out to be the same as that of a free Fermi gases of  $N$  particles with  $N_\uparrow = N_\downarrow = N/2$ , independently of  $U$ , at least for  $U > U^*$  with  $U^* < 0$  [62].

The asymptotic TSS can be easily determined from the results of Sec. III A, obtaining

$$\begin{aligned} \rho(\mathbf{x}, \ell, U, N) &= \ell^{-d\theta} [2S_p(\mathbf{X}, N/2) + O(\ell^{-\kappa})], \\ d_o(\mathbf{x}, \ell, U, N) &= \ell^{-2d\theta} [S_p(\mathbf{X}, N/2)^2 + O(\ell^{-\kappa})], \\ C(\mathbf{x}_1, \mathbf{x}_2, \ell, U, N) &= \ell^{-d\theta} [2E_p(\mathbf{X}_1, \mathbf{X}_2, N/2) + O(\ell^{-\kappa})], \\ G(\mathbf{x}_1, \mathbf{x}_2, \ell, U, N) &= \ell^{-2d\theta} [2Y_p(\mathbf{X}_1, \mathbf{X}_2, N/2) + O(\ell^{-\kappa})], \\ M(\mathbf{x}_1, \mathbf{x}_2, \ell, U, N) &= O(\ell^{-2d\theta - \kappa}), \\ P(\mathbf{x}_1, \mathbf{x}_2, \ell, U, N) &= \ell^{-2d\theta} [E_p(\mathbf{X}_1, \mathbf{X}_2, N/2)^2 + O(\ell^{-\kappa})], \end{aligned} \quad (43)$$

where the exponent of the leading power law are determined by the RG dimensions of the operators associated with the observables or the correlations, see Eq. (22). The presence of the on-site interaction induces scaling corrections with

$$\kappa = (d - 2)\theta. \quad (44)$$

For  $d = 3$  they dominate the scaling corrections expected within the lattice model of free spinless fermion, i.e. the Hubbard model with  $U = 0$ , which are relatively suppressed as  $O(\ell^{-2\theta})$ . [40]

The on-site interaction becomes marginal in 2D, thus a residual weak dependence on  $U$  is expected in the TSS limit, with at most logarithmic rescalings of the onsite interaction.

### 2. TSS in 1D systems

The relevance of the  $U$  term in 1D gives rise to non-trivial TSS limits, requiring an appropriate rescaling of the parameter  $U$ . Indeed, we expect the large- $\ell$  scaling behavior

$$\rho(x) \approx \ell^{-\theta} \mathcal{R}(X, U_r, N), \quad (45)$$

$$d_o(x) \approx \ell^{-2\theta} \mathcal{D}(X, U_r, N), \quad (46)$$

$$C(x_1, x_2) \approx \ell^{-\theta} \mathcal{C}(X_1, X_2, U_r, N), \quad (47)$$

$$G(x_1, x_2) \approx \ell^{-2\theta} \mathcal{G}(X_1, X_2, U_r, N), \quad (48)$$

$$M(x_1, x_2) \approx \ell^{-2\theta} \mathcal{M}(X_1, X_2, U_r, N), \quad (49)$$

$$P(x_1, x_2) \approx \ell^{-2\theta} \mathcal{P}(X_1, X_2, U_r, N), \quad (50)$$

where

$$X_i = x_i / \ell^\theta, \quad U_r = U \ell^\theta. \quad (51)$$

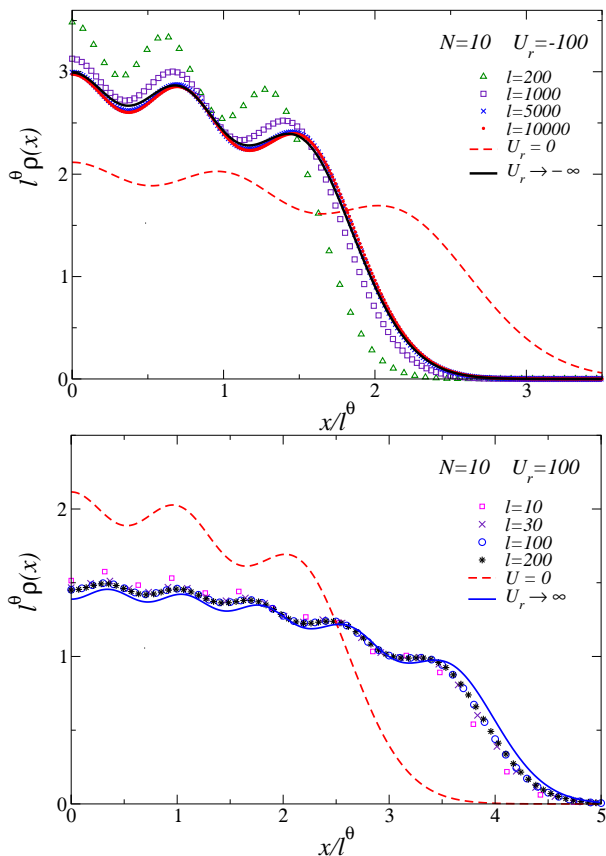


FIG. 2: (Color online) TSS of the particle density for  $N = 10$  particles, at fixed  $U_r \equiv Ul^\theta = -100$  (top) and  $U_r = 100$  (bottom). In both cases the data appear to converge to a nontrivial curve with increasing  $\ell$ , which are quite close to the  $U_r \rightarrow \infty$  and  $U_r \rightarrow -\infty$  limits respectively, cf. Eqs. (54) and (56), shown by the full lines. The dashed line is the  $U_r = 0$  curve for a free Fermi gas. Due to the reflection symmetry with respect the center of the trap, we show only data for  $x \geq 0$ .

$\theta$  is the same exponent of Eq. (21). These TSS behaviors are expected to be approached with power-law suppressed corrections. Of course, for  $U_r = 0$ , i.e. for a strictly vanishing  $U$ , we can derive the scaling functions from the results of Sec. III A, taking into account that an unpolarized free Fermi gases of  $N$  particles is equivalent to two independent spinless Fermi gases of  $N/2$  particles.

In order to check our predictions for the TSS behaviors, we present numerical DMRG [67] results for the 1D Hubbard model in the presence of a harmonic trap, for various values of  $U$ ,  $N$ , and  $\ell$ . DMRG simulations are performed for a chain of  $L$  sites with open boundary conditions. The size  $L$  is chosen sufficiently large to make finite-size effects negligible; in practice, we set  $L$  large enough to have  $\rho < 10^{-15}$  at the edges of the chain. The number of states  $M$  kept in the truncation is  $M \leq 1120$ ,

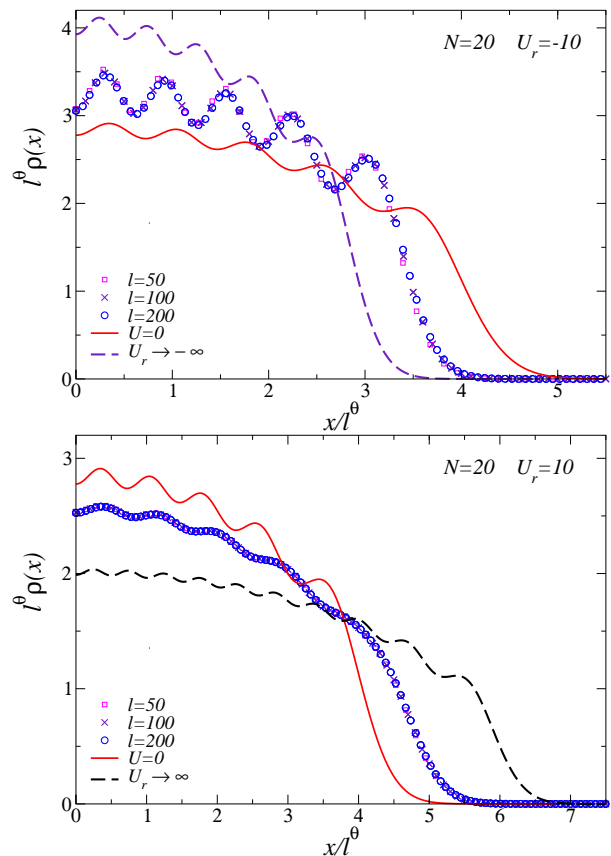


FIG. 3: (Color online) TSS of the particle density for  $N = 20$  particles,  $U_r = -10$  (top) and  $U_r = 10$  (bottom). The lines show the curves for  $U_r = 0$ ,  $U_r \rightarrow \infty$  and  $U_r \rightarrow -\infty$ .

which gives a maximum discarded weight below  $10^{-9}$ .<sup>1</sup> We use wavefunction prediction and exploit fully the conservation of the total number of particles of each species. The implicitly restarted Arnoldi method is used to diagonalize the Hamiltonian.

We note that, for large negative  $U$ , the strong on-site attraction tends to bunch together the particles in the middle of the trap: this effect reduces the chain length  $L$  needed to host all the particles, even down to  $O(N)$  in the limit  $U \rightarrow -\infty$ . Moreover, it also reduces the number of states kept in the DMRG truncation for a given accuracy. This fact allows us to get data for larger and larger trap size as the attractive interaction increases.

In Figs. 2 and 3 we show results for the particle density of systems with  $N = 10$  and  $N = 20$  particles, for some positive and negative values of the rescaled on-site interaction  $U_r \equiv Ul^\theta$ . They clearly confirm the TSS predicted by Eq. (45), indeed the data for  $\ell^\theta \rho(x)$  plotted versus

<sup>1</sup> In a few computations at large  $N$ , the maximum discarded weight is slightly larger than  $10^{-9}$ ; however the quality of the results is adequate for our needs: we estimate (by varying  $M$ ) that the truncation error is negligible in all figures presented.

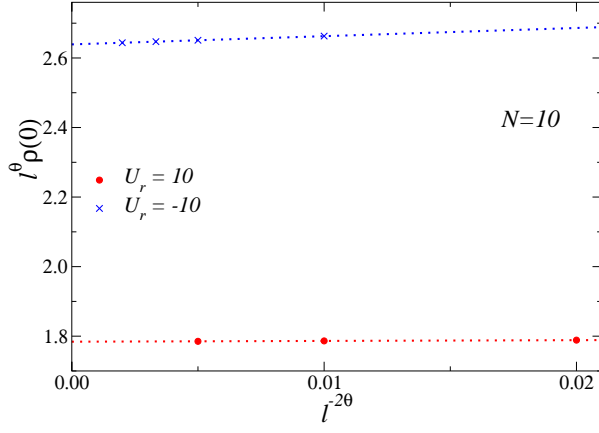


FIG. 4: (Color online) DMRG data of  $\ell^\theta \rho(0)$  vs  $\ell^{-2\theta}$  for  $N = 10$  and  $U_r = -10, 10$ . The dotted lines show linear fits, which support the  $O(\ell^{-2\theta})$  behavior of the corrections analogously to the free  $U = 0$  case.

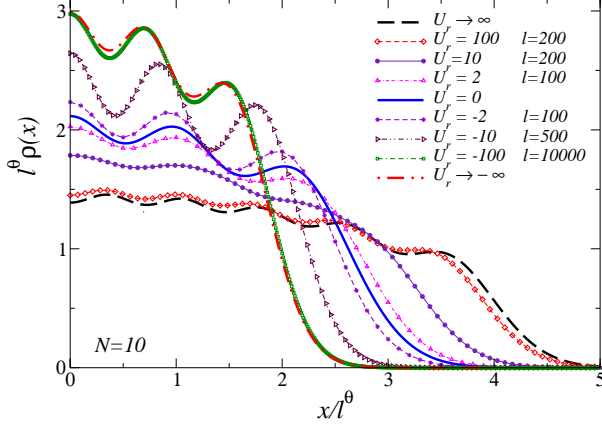


FIG. 5: (Color online) TSS functions of the particle density of  $N = 10$  particles, for various values of the scaling variable  $U_r$ . We report the exact curves for a free Fermi gas ( $U_r = 0$ ) and the limits  $U_r \rightarrow \pm\infty$ , cf. Eqs. (54) and (56). For the other values of  $U_r$  we plot the DMRG results for a sufficiently large trap size, providing already the asymptotic curves with high precision, as shown in Figs. 2 and 3 for some values of  $U_r$ .

$x/\ell^\theta$  appear to approach a limiting curve representing the TSS function  $\mathcal{R}(X, U_r, N)$  at the given value of  $U_r$  and  $N$ . The numerical results show that the asymptotic behavior is generally approached with  $O(\ell^{-2\theta})$  corrections relative to the leading behavior, as in the case of noninteracting fermion systems, see Sec. III A. Some DMRG data for the approach of the particle density at the origin to its asymptotic behavior are reported in Fig. 4. The amplitude of these corrections is significantly larger for attractive interactions, increasing with increasing  $|U_r|$ , requiring larger and larger trap sizes to observe the asymptotic behavior. For example the ratio between the amplitudes of the leading  $O(\ell^{-1})$  corrections at  $U_r = -10$  and  $U_r = 10$  is approximately 10.

The asymptotic TSS curves of the particle density

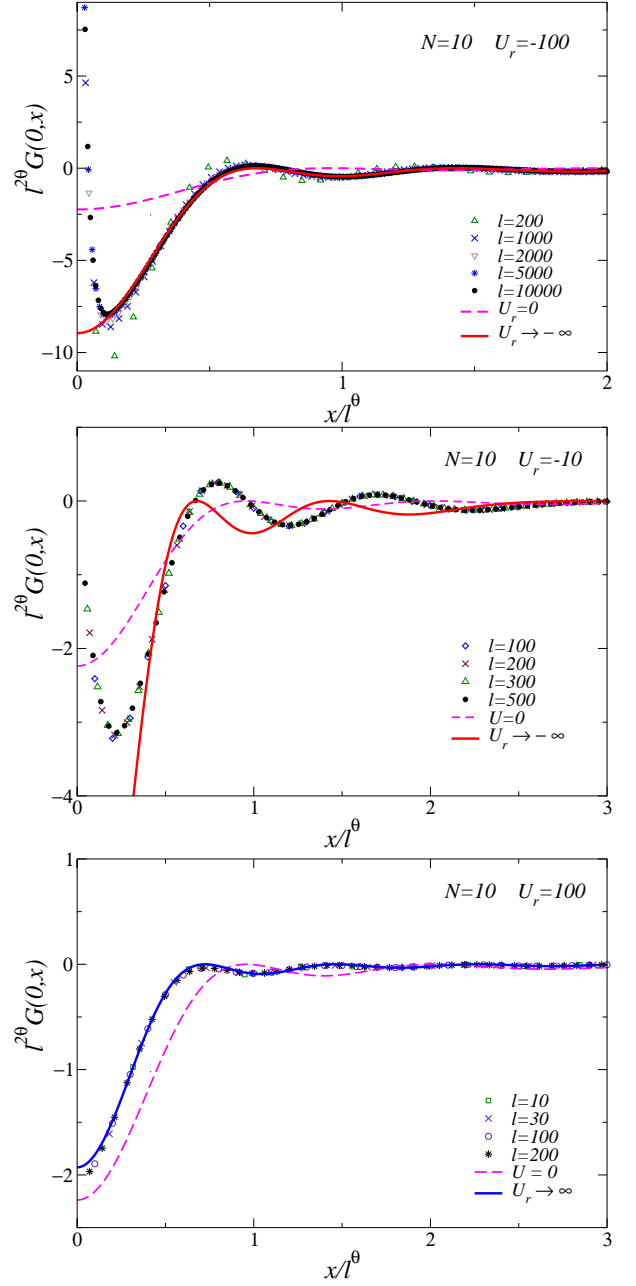


FIG. 6: (Color online) TSS of the density-density correlation  $G(0, x)$ , i.e. with a point fixed at the trap center, for  $N = 10$  particles, and  $U_r = -100, -10, 100$ . We plot  $\ell^{2\theta} G(0, x)$  vs  $x/\ell^\theta$ . The lines show the  $U = 0$  curve and the  $U_r \rightarrow \infty$  and  $U_r \rightarrow -\infty$  limits, cf. Eqs. (55) and (57).

clearly depend on the scaling variable  $U_r$ . In Fig. 5 we show them for  $N = 10$  and several values of  $U_r$ . As expected, they extend to larger regions when we pass from attractive to repulsive interactions. We also note that the scaling density shows  $N/2$  peaks for  $U_r \lesssim 10$ , while they become  $N$  for large  $U_r$ , see in particular the data for  $U_r = 100$ . As we shall discuss below, when varying  $U_r$  from the strongly attractive to the strongly repulsive regimes, the system experiences a crossover from a



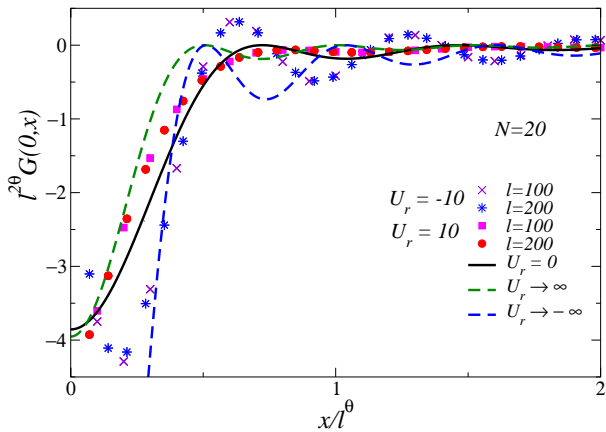


FIG. 7: (Color online)  $\ell^{2\theta} G(0, x)$  versus  $x/\ell^\theta$  for  $N = 20$  and  $U_r = -10, 10$ . The lines show the  $U_r = 0$  and  $U_r \rightarrow \pm\infty$  limits.

hard-core bosonic gas of  $N/2$  molecules to a free spinless fermion gas of  $N$  particles.

We also present results for the correlation functions introduced in Sec. II, in particular we consider correlation functions with a point fixed at the trap center  $x = 0$ . Figs. 6 and 7 show the scaling behavior of the connected density correlation function  $G(0, x)$ , for  $N = 10$  and  $N = 20$  respectively, and various values of  $U_r$ . The data nicely support the TSS Ansatz (48). In Fig. 8 we show results for the connected correlation  $M(0, x)$  between up and down density. TSS is also confirmed by the data of the one-particle correlation, see Fig. 9, and the pair correlation in Fig. 10. In particular, the quantities which are more sensitive to the correlation between up and down fermions, such as the up-down density correlation  $M(x, y)$  and the pair correlation  $P(x, y)$ , tend to become more and more significant with decreasing  $U_r$ , as expected because up and down fermions become more and more tightly correlated for large negative values of the on-site interaction. This is also shown by the behavior of the double occupancy shown in Fig. 11.

An important issue concerns the universality of the TSS reported in Eqs. (45-50). They are expected to be universal apart from a global multiplicative normalization, and normalizations of the arguments of TSS functions. More precisely, we expect that they are universal with respect to a large class of further short-ranged interaction terms, such as

$$H_{nn} = \sum_{\sigma, \sigma'} w_{\sigma\sigma'} \sum_{\langle xy \rangle} n_{\sigma x} n_{\sigma' y}. \quad (52)$$

Indeed,  $H_{nn}$  may only give rise to a change of the effective quartic coupling  $U$  (when adding  $H_{nn}$  to the Hubbard Hamiltonian, the effective relevant quartic coupling becomes  $U + 2w_{\uparrow\downarrow}$ ), and to further  $O(\ell^{-\theta})$  corrections, due to the fact that they introduce other irrelevant RG perturbations of RG dimension  $y_w = -d$  at the dilute fixed point.

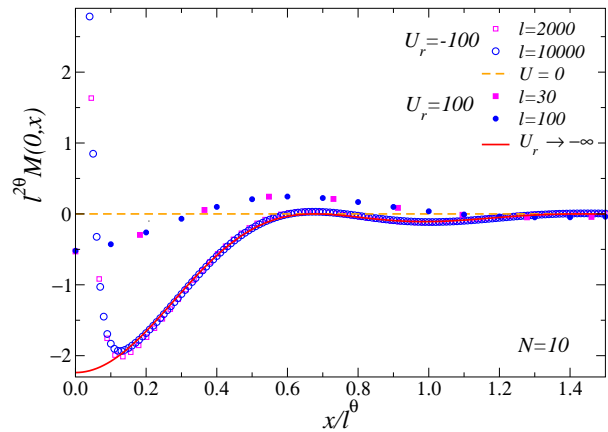


FIG. 8: (Color online) TSS of the correlation  $M(0, x) \equiv \langle n_{0\uparrow} n_{x\downarrow} \rangle_c$  for  $N = 10$  and  $U_r = -100, 100$ . We plot  $\ell^{2\theta} M(0, x)$  vs  $x/\ell^\theta$ . The full line represents the  $U_r \rightarrow -\infty$  limit given by Eq. (58).

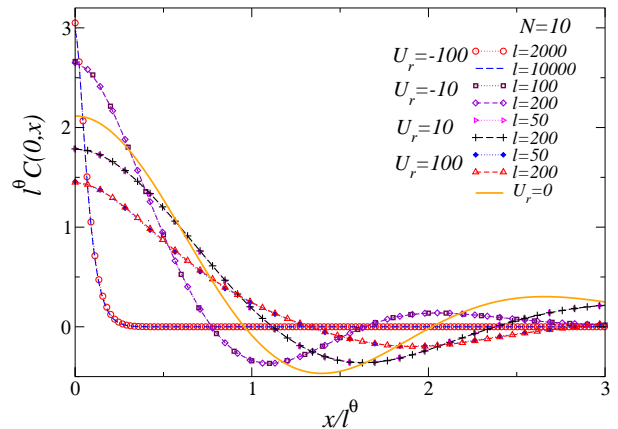


FIG. 9: (Color online) TSS of the one-particle correlation:  $\ell^\theta C(0, x)$  versus  $x/\ell^\theta$  for  $N = 10$  and various values of  $U_r$ .

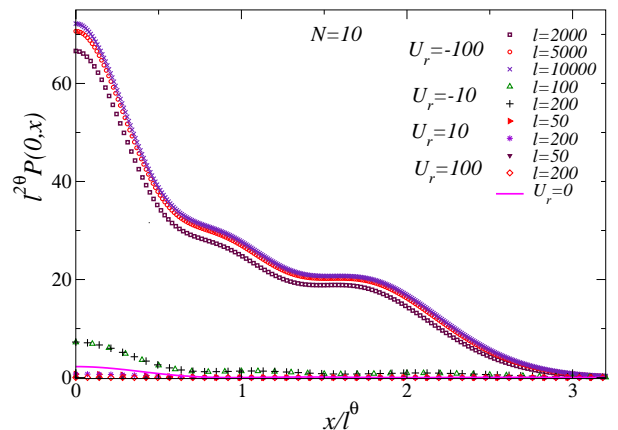


FIG. 10: (Color online) TSS of the pair correlation:  $\ell^{2\theta} P(0, x)$  versus  $x/\ell^\theta$  for  $N = 10$  and various values of  $U_r$ .



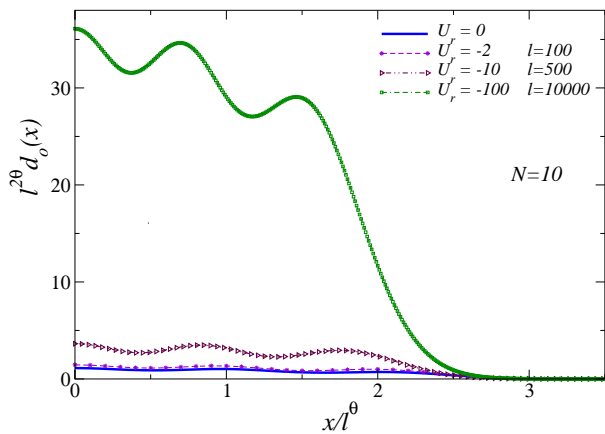


FIG. 11: (Color online) TSS functions of the double occupancy for  $N = 10$  and some values of  $U_r$ , obtained plotting  $l^{2\theta} d_o(x)$  versus  $x/l^\theta$ . Note that the double occupancy vanishes in the limit of strong repulsive interactions.

### 3. Crossover behavior as a function of the on-site interaction

It is important to note that the TSS limit corresponds to a continuum limit in the presence of the trap, i.e. it generally realizes a continuum quantum field theory in the presence of an inhomogeneous external field. In the case of the Hubbard model in the dilute regime, this continuum limit is given by the quantum field theory (16), replacing the constant  $\mu$  with a space-dependent potential  $\mu - V(\mathbf{x})$ . This implies that the TSS of the observables of the 1D trapped Hubbard model must approach the solutions of the continuous problem of fermions with contact interactions, which is also the so-called Gaudin-Yang (GY) model [68, 69], with equal number of up and down particles,  $N_\uparrow = N_\downarrow = N/2$ . The GY Hamiltonian of a trapped fermion gas can be written as

$$H_{\text{GY}} = \sum_{i=1}^N \left[ \frac{p_i^2}{2m} + V(x_i) \right] + g \sum_{i \neq j} \delta(x_i - x_j). \quad (53)$$

We expect that the TSS limit of the 1D Hubbard model at fixed  $N$  is related to the GY model with  $g \sim U_r$ . More precisely, the TSS functions entering formulas (45-50) are exactly given by corresponding quantities of the GY problem with a trap of unit size.

The equation of state of the homogenous GY model is exactly known for both repulsive and attractive zero-range interaction [68, 69]. It is characterized by different asymptotic regimes with respect to the effective dimensionless coupling  $\gamma \equiv g/\rho$ , where  $\rho$  is the particle density. At weak coupling  $\gamma \ll 1$  it behaves as a perfect Fermi gas; in the strongly repulsive regime,  $\gamma \gg 1$  the equation of state approaches that of spinless Fermi gas; in the strongly attractive regime  $\gamma \rightarrow -\infty$  and for unpolarized gases it matches that of a 1D gas of impenetrable bosons [70], more precisely hard-core bosonic molecules of fermion pairs [16, 71].

The relation between the TSS of the trapped Hubbard model and the continuum GY model can be exploited to determine the TSS functions of the particle density and its correlation, i.e.  $\mathcal{R}(X, U_r, N)$  and  $\mathcal{G}(X_1, X_2, U_r, N)$  respectively, in the strongly repulsive and attractive limits, i.e.  $U_r \rightarrow \infty$  and  $U_r \rightarrow -\infty$ .

We know that in the  $g \rightarrow \infty$  limit the particle density and its correlations of the GY model become identical to those of a gas of  $N$  spinless fermions [4, 72, 73]. This would imply that the  $U_r \rightarrow \infty$  limit of the TSS functions is

$$\mathcal{R}(X, U_r \rightarrow \infty, N) = S_p(X, N), \quad (54)$$

$$\mathcal{G}(X_1, X_2, U_r \rightarrow \infty, N) = Y_p(X_1, X_2, N), \quad (55)$$

where  $S_p$  and  $Y_p$  are the same functions entering the spinless free-fermion TSS, cf. Eqs. (27) and (33). Moreover, the TSS functions of the double occupancy and the pair correlation, i.e.  $\mathcal{D}(X, U_r, N)$  and  $\mathcal{P}(X_1, X_2, U_r, N)$ , defined in Eq. (46) and (50) respectively, trivially vanishes in the  $U_r \rightarrow \infty$  limit.

In the  $g \rightarrow -\infty$  limit the density properties of the GY model is expected to match that of an ensemble of hard-core  $N/2$  bosonic molecules constituted by up and down fermions. Indeed, with increasing attraction, the pairing becomes increasingly localized in space, and eventually the paired fermions form a tightly bound bosonic molecule. Actually, the results of Ref. [16] for harmonic traps, obtained by LDA, show that these bound states get trapped in a smaller region, with an effective trap size  $\ell_b = \ell/2$  in the strongly attractive limit. Thus, we expect that in the  $g \rightarrow -\infty$  limit the particle density of the unpolarized GY model (53) with a harmonic trap matches that of  $N/2$  hard-core doubly-charged bosons with an effective trap size  $\ell_b = \ell/2$ , which in turn can be mapped into a free gas of  $N/2$  spinless doubly-charged fermions in a harmonic trap of size  $\ell_b$ . On the basis of these arguments and using the results of Sec. III A, we conjecture the following  $U_r \rightarrow -\infty$  limit of the TSS functions for harmonic traps:

$$\mathcal{R}(X, U_r \rightarrow -\infty, N) = 2^{3/2} S_2(\sqrt{2}X, N/2), \quad (56)$$

$$\mathcal{G}(X_1, X_2, U_r \rightarrow -\infty, N) = 8Y_2(\sqrt{2}X_1, \sqrt{2}X_2, N/2). \quad (57)$$

Moreover, since fermion pairs are tightly bounded in the strongly attractive limit, we also predict

$$\mathcal{M}(X_1, X_2, U_r \rightarrow -\infty, N) = 2Y_2(\sqrt{2}X_1, \sqrt{2}X_2, N/2). \quad (58)$$

Using analogous arguments we may also expect that in this  $U_r \rightarrow -\infty$  limit the TSS function of the double occupancy becomes proportional to  $\mathcal{R}(X, U_r \rightarrow -\infty, N)$ . This is supported by the DMRG data by comparing the data of the double occupancy and the particle density for  $N = 10$  and  $U_r = -100$ , shown in Fig. 11 and the top Fig. 2 respectively. Moreover, in the same limit the TSS function of the pair correlation should get proportional to the one-particle correlation (density matrix) of a gas

of  $N/2$  hard-core bosons. This can be checked by comparing the  $U_r = -100$  data of Fig. 10 with the results of Ref. [40] for the one-particle correlation of hard-core Bose gases.

The curves corresponding to the  $U_r \rightarrow \pm\infty$  limits are shown in Figs. 2, 3, 5, 6, and 7 for both the particle density and its connected correlations. They are clearly approached by the data for large  $|U_r|$ , see in particular the results for  $N = 10$  in Figs. 2 and 6. Note that the limit  $U_r \rightarrow -\infty$  of the connected density-density correlations  $G$  and  $M$  is apparently approached nonuniformly at small distance. Indeed the data for  $U_r = -100$  shown in the top Fig. 6 appear to follow the asymptotic curve (57) for  $x/\ell^\theta \gtrsim 0.1$ , while at smaller distances they show a sudden departure where the correlation increases significantly. The comparison with the data for  $U_r = -10$ , see the middle Fig. 6, suggests that this occurs at smaller and smaller distances with increasing  $|U_r|$ , being likely related with the size of the molecules formed by the fermion pairs.

These data show that the dilute TSS of quantities related to the particle density of the trapped Hubbard model experience a smooth crossover from an effective hard-core bosonic gas of  $N/2$  molecules ( $U_r \rightarrow -\infty$ ) to an effective free gas of  $N$  spinless fermions ( $U_r \rightarrow \infty$ ), passing through two noninteracting fermion gases of  $N/2$  particles. In these 1D systems the formation of a gas of molecules of pair fermions has some analogies to the formation of a 3D molecule BEC and the BCS-BEC crossover for 3D Fermi systems, which has been recently observed in experiments with ultracold Fermi gases, see e.g. Refs. [3, 74–80].

Let us note that the  $U_r \rightarrow \infty$  limit of the TSS cannot be obtained by first taking the  $U \rightarrow \infty$  limit of the Hubbard model and then the large trap-size limit. Indeed, on the one hand, the  $U_r \rightarrow \infty$  limit of the TSS reproduces the  $g \rightarrow \infty$  limit of the continuous GY model, essentially given by a gas of free spinless fermions. On the other hand, the ground state of the Hubbard model in the  $U \rightarrow \infty$  limit should be obtained by filling the central  $N$  sites around the center of trap up to  $|x| \lesssim N/2$  (actually we expect some degeneration), without any particular scaling with respect to the trap size.

Analogous considerations apply to the limit  $U_r \rightarrow -\infty$ , which corresponds to a gas of  $N/2$  bosonic molecules with hard-core interactions. Indeed, the ground state of the trapped Hubbard model in the  $U \rightarrow -\infty$  limit of the Hubbard model (at any finite trap size  $\ell$ ) is just obtained by completely filling the central  $N/2$  sites around the center of trap (up to  $|x| \leq (N/2 - 1)/2$  if  $N/2$  is an odd number, in the case of even  $N/2$  there are two degenerate ground states filled for  $-N/4 \leq x < N/4$  and  $-N/4 < x \leq N/4$ ), without any particular scaling property with respect to the trap size.

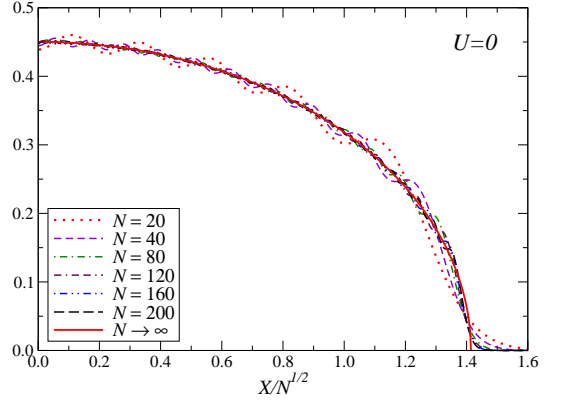


FIG. 12: (Color online) Large- $N$  scaling of the TSS function of the particle density of free Fermi gases:  $N^{-1/2}\mathcal{R}(X, U_r = 0, N)$  versus  $X/N^{1/2}$  for several values of  $N$ . The finite- $N$  curves, obtained using Eq. (28), clearly approach the large- $N$  limit  $\mathcal{R}_\infty(z)$ , cf. Eq. (60), with oscillations that get suppressed as  $1/N$ , in agreement with Eq. (60).

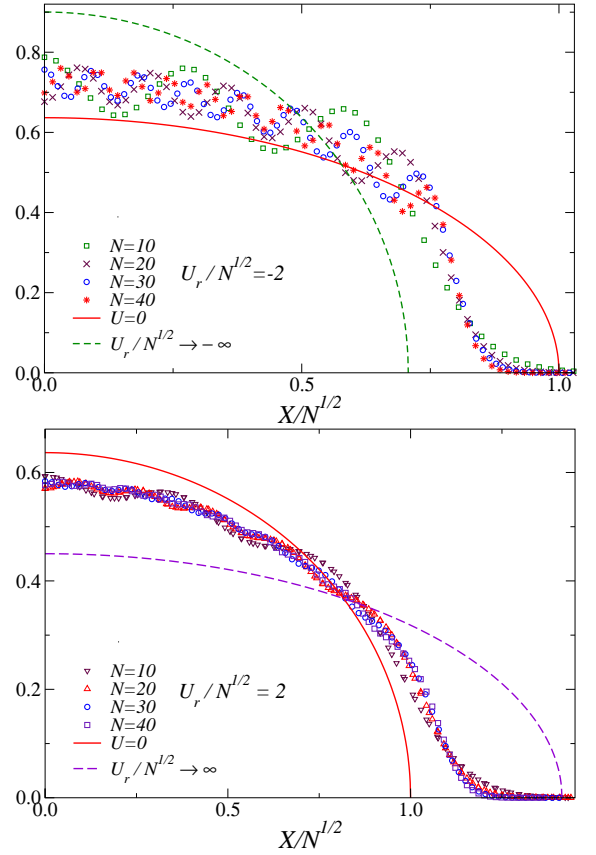


FIG. 13: (Color online) Large- $N$  scaling of the TSS function of the particle density:  $N^{-1/2}\mathcal{R}(X, U_r, N)$  versus  $X/N^{1/2}$  for  $U_r/N^{1/2} = -2$  (top) and  $U_r/N^{1/2} = 2$  (bottom). The TSS functions are derived from simulations with  $\ell = 100, 200$ , which are expected to be sufficiently large to effectively reproduce the  $\ell \rightarrow \infty$  limit. For comparison, we also show the asymptotic curve for  $U = 0$ , cf. Eq. (60), and the expected asymptotic curves for  $U_r/N^{1/2} \rightarrow \infty$  and  $U_r/N^{1/2} \rightarrow -\infty$ , given by Eq. (62) and (63) respectively.

### C. Large- $N$ limit of the dilute TSS functions

We now discuss the large- $N$  scaling behavior of the TSS function appearing on the r.h.s. of Eqs. (45-50). This also corresponds to studying the large- $N$  behavior of the GY model (53), which is reproduced by the asymptotic TSS functions of the Hubbard model in the large- $\ell$  limit.

On the basis of the results obtained at fixed  $N$  and  $U_r$ , we extend the Ansatz for the large- $N$  scaling of noninteracting Fermi gases, see the end of Sec. III A, to the 1D Hubbard model, by allowing for a large- $N$  rescaling of the on-site interaction. We argue that the TSS function of the particle density, cf. Eq. (45), behaves asymptotically as

$$\mathcal{R}(X, U_r, N) \approx N^{1/2} \mathcal{R}_\infty(X/N^{1/2}, U_r/N^{1/2}) \quad (59)$$

where  $\mathcal{R}_\infty(z, u)$  is a nontrivial scaling function, and power-law suppressed corrections are neglected. The large- $N$  rescaling of the on-site coupling  $U_r$  may be inferred by noting that in the continuum model (53) the strength  $g$  of the interaction should be compared with the density of the gas around the center of the trap, which is expected to increase as  $N^{1/2}$  with increasing  $N$  (keeping  $\ell$  fixed). This suggests that the effective coupling strength should be  $g/N^{1/2} \sim U_r/N^{1/2}$ . We mention that this rescaling of  $g$  was already considered in Ref. [48] for the continuum GY model. This large- $N$  rescaling may be also derived by requiring the consistency of this scaling behavior with the dilute limit  $N/\ell \rightarrow 0$  of the particle density as obtained by the LDA, see Sec. IV, which requires  $\rho = f_\rho(U, N/\ell, x/\ell)$  (taking into account that asymptotically  $N/\ell$  becomes a function of the chemical potential  $\mu$ ).

For  $U_r = 0$  we must recover the known results for spinless Fermi gases, [40, 81] taking into account that it corresponds to the large- $N$  limit of two identical Fermi gases of  $N/2$  particles. Thus, we must have

$$\mathcal{R}(X, 0, N) = N^{1/2} \left\{ \frac{2}{\pi} \sqrt{1-z^2} - \frac{(-1)^{N/2}}{N} \times \frac{\cos[N(z\sqrt{1-z^2} + \arcsin z)]}{2\pi(1-z^2)} + O(N^{-2}) \right\} \quad (60)$$

where  $z = X/N^{1/2}$ . In Fig. 12 we report some results for the noninteracting  $U = 0$  case, which show the above asymptotic behaviors with increasing  $N$ , including the oscillations arising from the  $O(1/N)$  term. Note that the  $O(1/N)$  corrections are singular at  $|z| = z_b = 1$  where the leading term vanishes. As explained at the end of Sec. III A, around  $z_b$  a different large- $N$  scaling sets in, so that at  $z = z_b$  the particle density behaves as

$$\rho(\pm z_b) = O(N^{1/6}), \quad (61)$$

instead of the  $O(N^{1/2})$  scaling for  $|z| < z_b$ . The difference with the value of  $z_b$  in Eq. (40) is just due to the fact that

here fermions have two spin components, thus we have  $N/2$  particles for each component.

The general interacting case shows similar behaviors. Fig. 13 shows results for the asymptotic large- $\ell$  scaling function  $\mathcal{R}(X, U_r, N)$  versus  $X/N^{1/2}$  at fixed  $U_r/N^{1/2} = -2, 2$ . They are obtained for a large trap size  $\ell$ , sufficiently large to reproduce the asymptotic TSS at fixed  $N$ . These results nicely support the expected large- $N$  scaling behavior (59). Again we observe the phenomenon of the restriction of the fermion cloud in the attractive regime. Moreover, we note the oscillations which should eventually get suppressed in the large- $N$  limit, likely as  $O(1/N)$  around the center of the trap analogously to the free case. The comparison of such oscillations for different values of  $U_r/N^{1/2}$  shows that their amplitudes are larger for attractive interactions.

We may also derive asymptotic behaviors in the limits  $u \equiv N^{-1/2}U_r \rightarrow \pm\infty$ , corresponding to the pictures derived in the limits  $U_r \rightarrow \pm\infty$  in Sec. III B 1. The  $u \rightarrow \infty$  limit corresponds to a free spinless fermi gas of  $N$  particles, thus

$$\mathcal{R}_\infty(z, u \rightarrow \infty) = \frac{2^{1/2}}{\pi} \sqrt{1 - \frac{z^2}{2}}. \quad (62)$$

On the other hand, the  $u \rightarrow -\infty$  is expected to reproduce the scaling density of a hard-core bosonic gas in an effective half trap, leading to

$$\mathcal{R}_\infty(z, u \rightarrow -\infty) = \frac{2^{3/2}}{\pi} \sqrt{1 - 2z^2}. \quad (63)$$

These curves are reported in Fig. 13. They provide the extreme behaviors when going from  $U_r/N^{1/2} \rightarrow \infty$  to  $U_r/N^{1/2} \rightarrow -\infty$ . In both  $U \rightarrow \pm\infty$  limits the corrections are again expected to be  $1/N$ , since they the corresponding particle densities map into those of free Fermi systems.

Like the noninteracting  $U = 0$  case, see Sec. III A, the one-point correlation and the connected density correlation scale differently with respect to the distance from the trap center, as

$$\mathcal{C}(X_1, X_2, U_r, N) \approx N^{1/2} \mathcal{C}_\infty(N^{1/2} X_i, U_r/N^{1/2}), \quad (64)$$

$$\mathcal{G}(X_1, X_2, U_r, N) \approx N \mathcal{G}_\infty(N^{1/2} X_i, U_r/N^{1/2}). \quad (65)$$

Clear evidence of this scaling behavior is shown by the DMRG data, see e.g. Fig. 14 which shows data for  $N^{-1}\mathcal{G}(0, X, U_r, N)$  versus  $N^{1/2}X$  keeping  $U_r/N^{1/2}$  fixed.

## IV. THE TRAP THERMODYNAMIC LIMIT

We now consider another large- $\ell$  limit, the so-called thermodynamic limit in a trap, i.e.  $\ell \rightarrow \infty$ ,  $N \rightarrow \infty$  keeping the ratio

$$v \equiv N/\ell^d \quad (66)$$

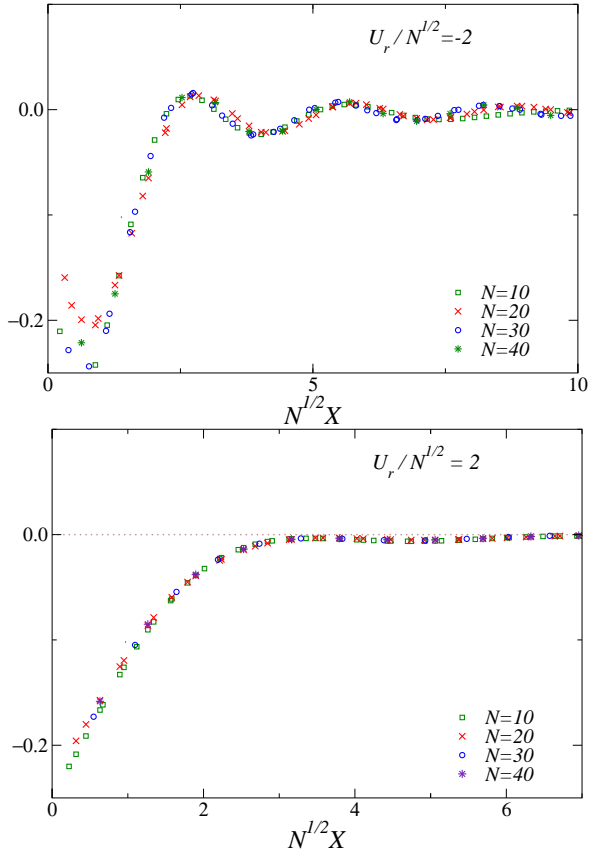


FIG. 14: (Color online) Large- $N$  scaling of the TSS function of the connected density correlation:  $N^{-1}\mathcal{G}(0, X, U_r, N)$  versus  $N^{1/2}X$  keeping  $u \equiv U_r/N^{1/2}$  fixed, for  $u = -2$  (top) and  $u = 2$  (bottom). The data for negative  $U$  appear to converge more slowly to their large- $N$  limit.

fixed. Note that  $v$  becomes proportional to the filling  $N/V$  in the  $p \rightarrow \infty$  limit of the trapping potential, cf. Eq. (5) (in 1D the filling would be  $f = v/2$ ). The above thermodynamic limit in a trap can be realized by introducing a chemical-potential term, cf. Eq. (7). Indeed,  $v$  and  $\mu$  must be asymptotically related, i.e.  $v = \Upsilon(\mu)$ . We shall show that the function  $\Upsilon(\mu)$  can be exactly determined by LDA.

Notice that the asymptotic trap-size scaling keeping  $v$  fixed does not reproduce the continuum limit given by the GY model, essentially because  $\ell$  is considered in units of the lattice spacing.

### A. Accuracy of the LDA of the particle density

In the presence of a space-dependent confining potential, LDA estimates the space-dependent particle density by the value of the particle density  $\rho_h(U, \mu)$  of the homogeneous system at the effective chemical potential

$$\mu_{\text{eff}}(\mathbf{x}/\ell) \equiv \mu - V(\mathbf{x}) = \mu - (\mathbf{x}/\ell)^2. \quad (67)$$

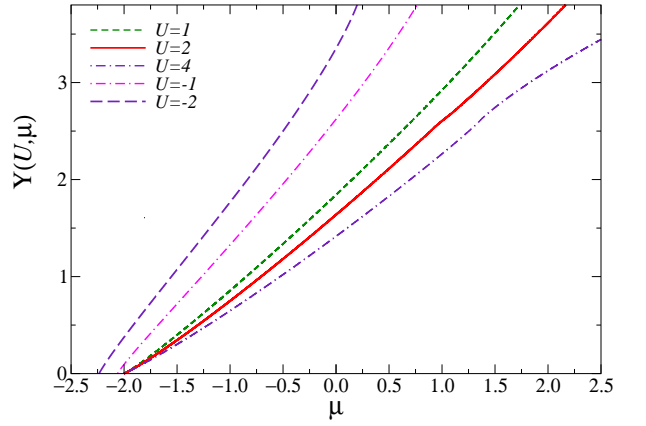


FIG. 15: (Color online) The function  $\Upsilon(U, \mu)$  providing the asymptotic relation between  $v \equiv N/\ell$  and  $\mu$ , cf. Eq. (71), for various values of  $U$ .

This implies that the LDA particle density is a function of the ratio  $\mathbf{x}/\ell$ . Indeed, we have

$$\rho(\mathbf{x}, \ell, U, \mu) \approx \tilde{\rho}_{\text{lda}}(\mathbf{x}/\ell, U, \mu) \equiv \rho_h[U, \mu_{\text{eff}}(\mathbf{x}/\ell)]. \quad (68)$$

LDA usually provides a good approximation of the particle density when the inhomogeneous external potential is sufficiently smooth. Therefore, it is expected to provide better and better approximations with increasing the trap size. However, substantial deviations may be present in the case the system develops long-range correlations.

LDA has been largely employed in studies of inhomogeneous fermion systems, and in particular for 1D systems [2, 4, 7, 9, 10, 13, 14, 16, 17, 19–27, 41–43, 48]. However, an analysis of the deviations from LDA is called for, to get a robust confidence of its results. We investigate this issue in the trapped 1D Hubbard model (4), where the particle density  $\rho_h(U, \mu)$  of the homogeneous system can be exactly computed using the Bethe-Ansatz techniques, as a function of  $U$  and  $\mu$ . [59] Some details are reported in App. B. This allows us to check the accuracy of LDA with the Hubbard model, and quantify the deviations of very accurate (practically exact) numerical results obtained by DMRG simulations.

Assuming that LDA provides the exact large- $\ell$  limit, we may derive the asymptotic relation between the particle number and the chemical potential:

$$\begin{aligned} v \equiv N/\ell &\approx \ell^{-1} \sum_x \tilde{\rho}_{\text{lda}}(x/\ell, U, \mu_v) \\ &\approx \int_{-\infty}^{\infty} dz \tilde{\rho}_{\text{lda}}(z, U, \mu_v) = \Upsilon(U, \mu_v). \end{aligned} \quad (69)$$

In Fig. 15 we show the function  $\Upsilon(U, \mu)$  for some values of  $U$ . We use this relation to derive the chemical potential corresponding to the value  $v$  we are interested in. In practice, for a given value of  $v$ , we consider the LDA

$$\rho_{\text{lda}}(x, U, v) \equiv \tilde{\rho}_{\text{lda}}(x, U, \mu_v) \quad (70)$$

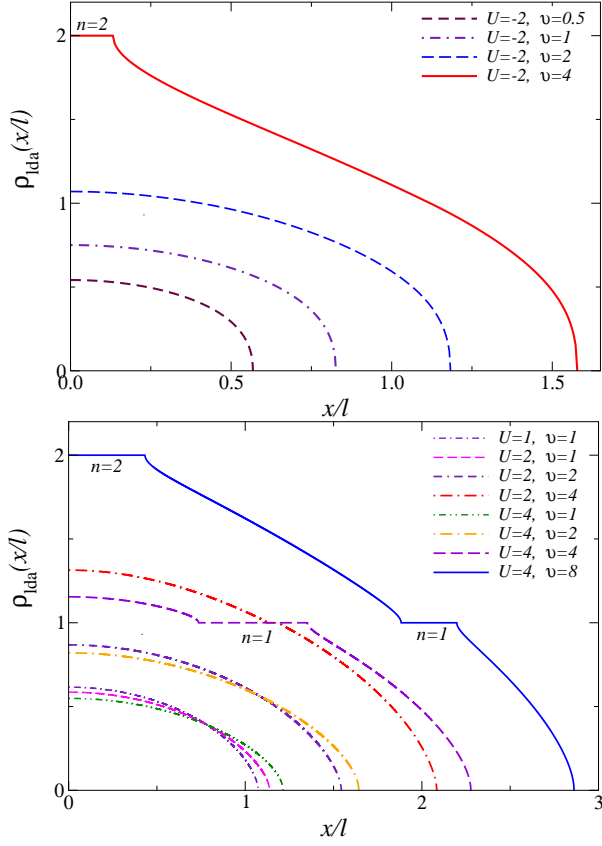


FIG. 16: (Color online) LDA of the particle density for some negative (top) and positive (bottom) values of  $U$ . Since the curves are symmetric for  $x \rightarrow -x$ , we show only them for  $x \geq 0$ . Note that the  $n = 1$  and  $n = 2$  plateaus for some of the curves shown in the figures, which correspond to the Mott phases of Fig. 1.

with  $\mu_v$  obtained using the equation

$$v = \Upsilon(U, \mu_v). \quad (71)$$

The eventual consistency of the results will support this work hypothesis.

Before showing results for the Hubbard model, we note that for  $U = 0$  we must recover the known results for free fermion lattice systems. As shown in Ref. [39], the LDA of the particle density of 1D hard-core bosons, equivalent to a free spinless Fermi gas, provides the asymptotic behavior in the large- $\ell$  limit keeping  $x/\ell$  fixed. This also applies to the unpolarized Hubbard model for  $U = 0$ , for which we have two identical free spinless Fermi gases with half particles. Thus, the LDA of the particle density at  $U = 0$  reads

$$\rho_{\text{lda}}(x, U = 0, v) = 2 \rho_{\text{lda0}}(x, v/2) \quad (72)$$

where

$$\rho_{\text{lda0}}(x, v) = \tilde{\rho}_{\text{lda0}}(x, \mu_v) = \begin{cases} 0 & \text{for } \mu_{\text{eff}}(x) < -2, \\ (1/\pi) \arccos[-\mu_{\text{eff}}(x)/2] & \text{for } -2 \leq \mu_{\text{eff}}(x) \leq 2, \\ 1 & \text{for } \mu_{\text{eff}}(x) > 2, \end{cases} \quad (73)$$

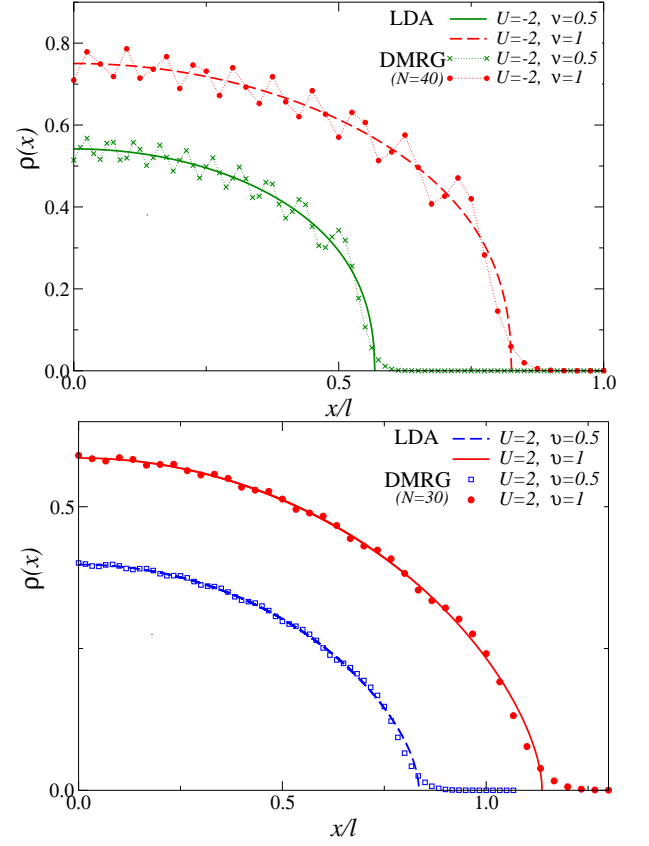


FIG. 17: (Color online) Comparison of DMRG and LDA results of the particle density, for  $U = -2$  (top) and  $U = 2$  (bottom) and  $v = 0.5, 1$ . Since the curves are symmetric for  $x \rightarrow -x$ , we show only data for  $x \geq 0$ .

with  $\mu_{\text{eff}} = \mu_v - V(x)$ , and  $\mu_v$  is related to the ratio  $v \equiv N/\ell$  by

$$v = \int_{-\infty}^{\infty} dx \tilde{\rho}_{\text{lda0}}(x, \mu_v). \quad (74)$$

The corrections to the relation (69) turn out to be  $O(\ell^{-1})$  for free Fermi gases, thus for the Hubbard model at  $U = 0$ . We expect that this fact extends to nonzero on-site interactions.

Fig. 16 shows some results for the LDA of the particle density, for some values of  $v$  and  $U$ , derived using the Bethe Ansatz for the homogenous system, see App. B, and assuming Eq. (69). Depending on the values of  $v$  and  $U$ , the curves show plateaus at integer values corresponding to the Mott phases of the phase diagram shown in Fig. 1. Analogous results have been also reported in Ref. [13, 82], by quantum Monte Carlo and DMRG simulations. In Fig. 17 we compare the LDA curves with the DMRG results for  $U = 2$  and  $v = 1/2, 1$ . Analogous results are derived for other values of  $U$  and  $v$ . We note that the agreement is satisfactory, but deviations are clearly observed, in particular at the boundary of the fermion cloud. We also note that the oscillations around the asymptotic curve are larger in the case of attractive



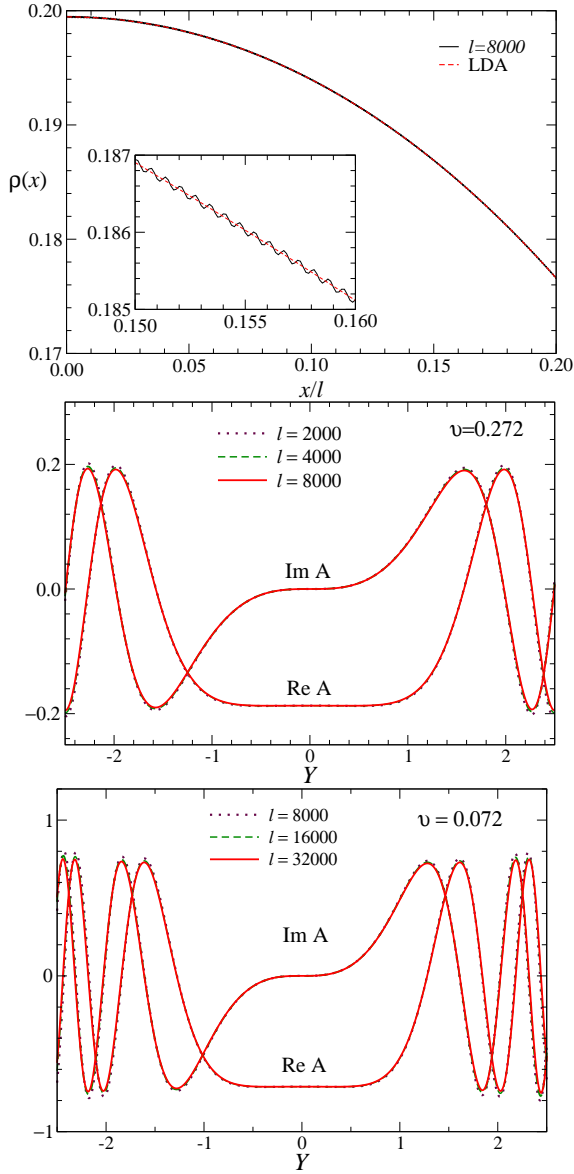


FIG. 18: (Color online) The top figure shows the particle density for  $\nu = 0.272$  and  $\ell = 8000$  and its LDA approximation (the inset is necessary to observe the tiny differences). The other figures show the real and imaginary part of the complex function  $A(Y, \nu)$  in Eq. (76) for two values of  $\nu$ ,  $\nu = 0.272$  and  $\nu = 0.072$  corresponding respectively to  $q = 0.6399\dots$  and  $q = 1.253\dots$

interactions.

In order to characterize the deviations from LDA, whether they really vanish in the large- $\ell$  limit and how they get suppressed if LDA becomes asymptotically exact, we consider the difference

$$\Delta\rho \equiv \rho(x, \ell, U, \nu) - \rho_{\text{lda}}(x/\ell, U, \nu). \quad (75)$$

We investigate whether and how such a difference gets suppressed in the large trap-size limit. In the following we consider the case in which the whole trapped sys-

tem is within the metallic phase, but the analysis can be straightforwardly extended to the other possible cases.

In the case of free Fermi systems, i.e.  $U = 0$ , the difference  $\Delta\rho$  vanishes as  $O(\ell^{-1})$  around the center of the trap, with a quite intricate scaling within the metallic phase, as shown by the results of Ref. [39] for free fermion systems (or equivalently hard-core Bose-Hubbard systems) at fixed chemical potential. In the case of fixed ratio  $N/\ell$ , an educated guess for its asymptotic behavior turns out to be

$$\ell \Delta\rho(x, \ell, U = 0, \nu) \approx \text{Re} [A(Y, \nu)e^{iqx}] + o(1), \quad (76)$$

$$Y = x\ell^{-2/3}, \quad q = \pi\rho_{\text{lda}}(0, 0, \nu),$$

where  $A$  is a nontrivial complex function. This is supported by numerical results up to very large trap size, up to  $\ell = O(10^4)$  by exact diagonalization methods, as shown by Fig. 18 which shows results for some values of  $\nu$ . This is consistent with the analysis of free fermion systems (or equivalently hard-core Bose-Hubbard systems) at fixed chemical potential reported in Ref. [39]. Moreover, free Fermi systems show an anomalous behavior at the boundaries of the trap, where the LDA of the particle density vanishes, and much larger  $O(\ell^{-1/3})$  corrections arise [39, 49]. An interesting issue is whether these features extend to the interacting  $|U| > 0$  case.

For this purpose we present DMRG results at fixed  $\nu \equiv N/\ell$  and various values of  $U$ . Figs. 19 show some data of  $\ell\Delta\rho$  versus  $x/\ell$  for  $\nu = 1$  and  $U = \pm 2$ . Analogous results are obtained for other values of  $\nu$  and/or  $U$ . The difference  $\Delta\rho(x)$ , defined in Eq. (75), does not show a simple scaling behavior. However it shows most features of the free Fermi gas. Indeed, around the center of the trap the product  $\ell\Delta\rho$  shows an oscillating behavior with an almost constant amplitude, indicating that  $\Delta\rho$  gets suppressed as  $O(\ell^{-1})$  around the center of the trap. Such oscillations were already reported and discussed in the literature, see e.g. Refs. [48, 83]. Moreover, the number  $n_{\text{peak}}$  of peaks turns out to increase proportionally to  $\ell$  as suggested by the phase term in Eq. (76) (more precisely at  $U = -2, 2$  we count  $n_{\text{peak}} \approx N/2 = \nu\ell/2$ ). We also note that the deviations from LDA get further suppressed, effectively as  $O(\ell^{-2})$ , by averaging the oscillations around the center of the trap, in a relatively large space interval sufficiently far from the boundaries, for  $x/\ell \lesssim 0.2$  say. Our DMRG results for the Hubbard model are not sufficiently asymptotic to disentangle terms scaling differently as in Eq. (76).

We finally mention that the connected density-density correlation  $G(0, x)$  turns out to vanish after a few lattice spacings, without showing any particular dependence on the trap size, see e.g. Fig. 20.

## B. Scaling behavior at the boundary of the trap

As already mentioned, Figs. 19 show significant deviations at the boundary of the cloud, where the amplitude

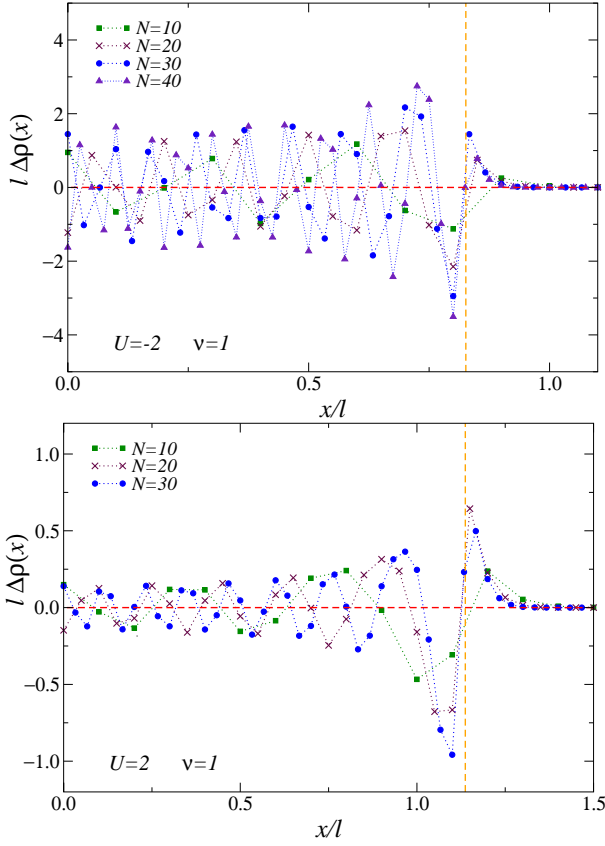


FIG. 19: (Color online) DMRG data for the product  $\ell\Delta\rho(x)$ , where  $\Delta\rho(x)$  is the difference of the particle density and its LDA, for  $\nu = 1$ ,  $U = -2$  (top) and  $U = 2$  (bottom). The vertical dashed line indicates the value  $X_0 = x_0/\ell$  where the LDA of the particle density vanishes.

of the fluctuations do not appear constant by clearly increase. The data indicate that around the boundaries of the fermion cloud the behavior is substantially different, and the deviations may have a different origin. They can be explained as an effect of the metal-to-vacuum transition occurring at the boundary of the cloud. Indeed, for repulsive interactions, at the spatial points corresponding to  $\mu_{\text{eff}}(x) \approx \mu_0 = -2$  the system effectively passes from the vacuum [where  $\mu_{\text{eff}}(x) \lesssim -2$  for  $U > 0$ ] to the metallic [where  $\mu_{\text{eff}}(x) \gtrsim -2$ ] space region. We thus expect that, for generic values of  $\mu$  and  $U > 0$ , the regions around  $x_0/\ell = \pm X_0$ , with

$$X_0 = \sqrt{2 + \mu}, \quad \mu_{\text{eff}}(X_0) = -2, \quad (77)$$

develop quantum critical modes. But we must take into account that this occurs in the presence of an external space-dependent field. The effective chemical potential can be expanded around  $x_0$  as

$$\mu_{\text{eff}} = \mu - (x/\ell)^2 = -2 - 2X_0 \frac{x - x_0}{\ell} + O[(x - x_0)^2]. \quad (78)$$

Thus, the behavior around  $x_0$  is essentially analogous to that arising at the vacuum-to-metal transition in the

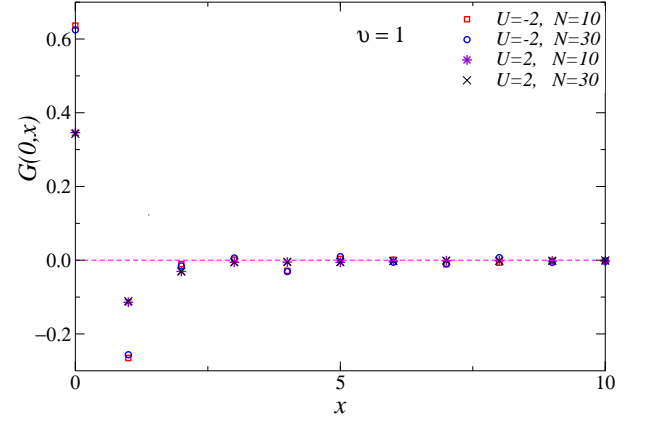


FIG. 20: (Color online) Results for the connected density-density correlation  $G(0,x)$  at  $U = \pm 2$  and  $\nu = 1$ . For each value of  $U$  the  $N = 10$  and  $N = 30$  data vary very little.

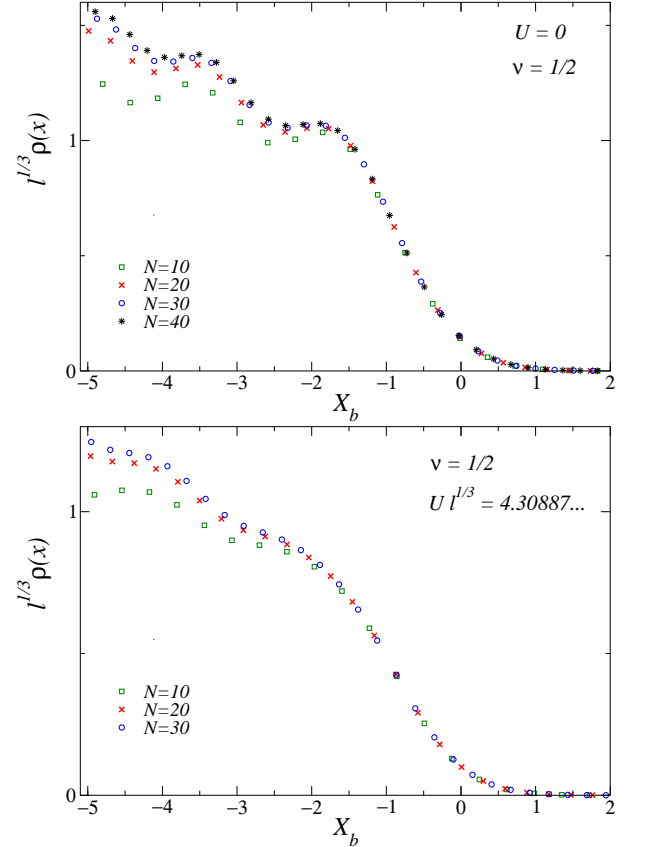


FIG. 21: (Color online) Scaling at the boundaries of the cloud:  $\ell^{1/3}\rho(x)$  versus  $X_b \equiv (x - x_0)/\ell^{1/3}$  for  $U = 0$  (top) and  $U\ell^{1/3} = 4.30887\dots$  (bottom).

presence of a linear potential  $V_l \sim r/\ell$ . Around  $x_0$ , critical modes should appear with length scale  $\xi \sim \ell^\sigma$ , where  $\sigma$  is the exponent associated with a linear external potential. Thus, by replacing  $p = 1$  in Eq. (21), we obtain  $\sigma = 1/3$ . We expect that around  $x = x_0$  the particle



density shows the scaling behavior

$$\rho(x; U, \ell, v) \approx \ell^{-1/3} f_\rho(X_b, U_b), \quad (79)$$

$$X_b = (x - x_0)/\ell^{1/3}, \quad U_b = U\ell^{1/3}. \quad (80)$$

A similar scaling behavior is also expected for the correlation functions around  $x_0$ . For example the connected density correlation is expected to scale as

$$G(x_0, x) = \ell^{-2/3} f_g(X_b, U_b). \quad (81)$$

An analogous behavior is found in trapped bosonic systems with repulsive interaction, see e.g. the results of Refs. [39, 49, 51]. The above scaling behaviors are nicely confirmed by the DMRG data, see e.g. Figs. 21, where we show results for the particle density keeping  $v \equiv N/\ell$  and  $U_b = U\ell^{1/3}$  fixed.

The scaling (79) implies that  $\rho(x)$  gets roughly suppressed as  $\ell^{-1/3}$  at  $x_0$  where  $\rho_{\text{lda}}$  vanishes (assuming that  $f_\rho(0, u) \sim \text{const}$  for  $u \rightarrow \pm\infty$ ). Therefore, corrections to LDA are  $O(\ell^{-1/3})$  around the boundary, thus much less suppressed than those around the center of the trap, which are  $O(\ell^{-1})$  and oscillating. Note that this anomalous scaling behavior at the boundaries does not necessarily affect the corrections between the total particle number and its LDA approximation, cf. Eq. (69), which are expected to be suppressed as  $O(\ell^{-1})$ . Indeed, although corrections to the LDA of the particle density are  $O(\ell^{-1/3})$  around the boundary of the trap, the region where such behavior is observed shrinks as  $O(\ell^{-2/3})$  in terms of  $x/\ell$  (which means that this boundary critical region enlarges as  $\ell^{1/3}$  around  $x_0$ ).

The above edge scaling behaviors are expected to be universal apart from a multiplicative constant and normalizations of the arguments of the scaling functions. They are universal with respect to changes of the chemical potential  $\mu$ , thus  $v$ , and microscopic short-ranged interactions, for example adding the nearest-neighbor interaction (52), essentially because they are controlled by the dilute fixed point of the field theory (16) in the presence of an external linear field.

We also note that analogous phenomena are expected around the space region corresponding to a transition between metallic and Mott phases, at the end of the plateaus of the particle-density curves shown in Fig. 16. Such a transition is controlled by the same RG exponents of the dilute fixed points, cf. Eqs. (17) and (21), which can be inferred from the exact solution for the homogenous system. Thus scaling equations analogous to Eqs. (79-81) are expected to apply around the edges of the density plateaus.

Analogous scaling behaviors are also expected in higher-dimensional fermionic systems, at the boundaries of their trap. For example, in 3D systems with a rotational invariant trap, the radial space dependence of the particle density around the boundary of the trap should behave

$$\rho(r; U, \ell, v) \approx \ell^{-d/3} f_\rho(R_b), \quad (82)$$

where  $R_b = (r - r_0)/\ell^{1/3}$  and  $r_0$  is the space distance where the particle density vanishes asymptotically. Note the independence of  $U$  of the leading scaling behavior, due to the fact that the quartic coupling is irrelevant at the three-dimensional dilute fixed point, see Sec. III B.

## V. SUMMARY AND CONCLUSIONS

We study the effects of an inhomogeneous trap in fermion systems described by the lattice Hubbard model with an external confining potential, in the zero-temperature limit. This issue is of experimental relevance because these systems are investigated in experiments with ultracold atoms, see e.g. Refs. [1–3]. Indeed an important feature of these experiments is the presence of a confining force, which traps the atoms within a limited spatial region.

We investigate the scaling behavior of the ground state of unpolarized systems, i.e. with zero global spin, when varying the size  $\ell$  of the trap. The trap size  $\ell$  is naturally defined by writing the external harmonic potential as  $V(\mathbf{x}) = t|\mathbf{x}|^2/\ell^2$ , cf. Eq. (6), where  $t$  is the kinetic constant (tunneling rate) of the Hubbard model (1). We mostly consider 1D systems, with both attractive and repulsive interactions, in the dilute regime when the trap size  $\ell$  gets large keeping the particle number  $N$  fixed, and in the *trap thermodynamic* limit defined as the large- $N$  limit keeping the ratio  $v \equiv N/\ell$  fixed. We discuss the universal behavior of several observables, such as the particle density, double occupancy, density-density correlation, one-point correlation, and pair correlation.

For a lattice system of  $N$  fermion particles with short-range interactions, such as the Hubbard model, the trap-size dependence in the dilute regime shows universal scaling behaviors, which can be described in the framework of the TSS theory [5, 6]. The universal features of the TSS in the dilute regime of Hubbard models are derived by a RG analysis of the various relevant perturbations at the dilute fixed point. In particular, TSS is controlled by the trap exponent  $\theta$ , cf. Eq. (21), related to the RG perturbation arising from the trapping potential. This implies that spatial coordinates  $\mathbf{x}$  must be rescaled as  $\mathbf{X} = \mathbf{x}/\ell^\theta$  to get a nontrivial TSS limit when  $\ell \rightarrow \infty$ . For harmonic traps, which is the relevant case in most experiments,  $\theta = 1/2$  in any spatial dimensions.

In three dimensions the dilute fixed point is stable with respect to the on-site interaction, thus the TSS behavior approaches that of a free Fermi gas, cf. Eqs. (43), independently of  $U$ . The on-site interaction gives only rise to  $O(\ell^{-\theta})$  relative corrections. On the other hand, in the 1D case the on-site interaction turns out to be relevant. Thus the TSS in the dilute regime also requires a nontrivial rescaling of the on-site coupling  $U$ , indeed the corresponding scaling variable turns out to be  $U_\tau = U\ell^\theta$ . This RG analysis leads to the universal TSS reported in Eqs. (45-50). We argue that the leading TSS behavior reproduces the particle density and correlations of a

1D Fermi gas defined in the continuum, given by the so-called Gaudin-Yang model [68, 69] in the presence of a trapping potential, cf. Eq. (53), with  $g \sim U_r$ .

In order to check, and further characterize, the TSS of the 1D Hubbard model at fixed  $N$ , we present results of DMRG simulations for several values of  $N$ , the on-site interactions, and the trap size  $\ell$  of the harmonic trap. The DMRG results are in full agreement with the TSS predictions. In particular, the data show that the TSS functions of the particle density and density-density correlation crossover among different asymptotic regimes where these quantities can be exactly computed, i.e. for strongly repulsive interactions where they approach those of a spinless Fermi gas, for weak interactions those of a free Fermi gas, and for strongly attractive interactions they match those of a gas of hard-core bosonic molecules. In these 1D systems the formation of a gas of molecules of pair fermions presents some analogies to the formation of a 3D molecule BEC and the BCS-BEC crossover for 3D Fermi systems, which has been recently observed in experiments with ultracold Fermi gases, see e.g. Refs. [3, 74–80].

The large- $N$  behavior of the TSS functions show a further nontrivial large- $N$  scaling. We argue that the space dependence of the particle density and the correlations show a substantially different scaling behavior, see Eqs. (59), (64), and (65). Indeed, while the large- $N$  scaling behavior of the particle density is realized keeping  $X/N^{1/2}$  fixed, the large- $N$  behavior of the TSS functions of the correlations is obtained keeping  $N^{1/2}X$  fixed, thus remaining significant only at short distance.

The 1D Hubbard model in the trap thermodynamic limit is asymptotically equivalent to introducing a chemical-potential term, as in Eq. (7). We address the issue of the accuracy of the LDA, which approximates the space-dependent particle density in a trap by the particle density of the homogenous system at the corresponding value of the effective chemical potential. LDA is routinely used in the analyses of the numerical and experimental data of inhomogeneous particle systems. However, a quantitative analysis of the deviations from LDA, and therefore of its accuracy, is required to get a robust confidence of its results, especially when the actual trap size is not very large and/or the system is close to criticality.

In the 1D Hubbard model the validity of LDA can be accurately checked because the particle density of homogenous systems can be exactly computed by Bethe-Ansatz methods. We show that LDA becomes exact in the large trap-size limit keeping  $x/\ell$  fixed, with power-law suppressed corrections. When the trapped system is in the metallic phase, the corrections to LDA turn out to be  $O(\ell^{-1})$  and oscillating around the center of the trap. Actually they may be further suppressed by appropriate averages around the center of the trap, likely to  $O(\ell^{-2})$ . However, they become much larger at the boundary of the fermion cloud, where they get suppressed as  $O(\ell^{-1/3})$  only. Such an anomalous behavior at the boundary of the trapped fermion cloud is explained, and described, by a

quantum critical behavior at the metal-to-vacuum transition occurring at the boundaries of the trap.

In our study we consider in particular the observables related to the particle density, double occupancy, and their correlations, determining the scaling behaviors of their space dependence along the trap. These features can be experimentally investigated by in situ imaging techniques for atomic quantum gases, [28, 84, 85] which allow to probe the spatial dependence of the particle density, and also density fluctuations and density-density correlations, see, e.g., Refs. [86–88].

The study of the scaling behavior of trapped interacting Fermi systems may be extended considering also unbalanced systems. In this case attractive interactions give rise to new states such as the Fulde-Ferrel-Larkin-Ovchinnikov (FFLO) state [89], in which an unbalance in the populations with different spin leads to the formation of Cooper pairs with nonzero momentum. Experimental evidence of such states has been recently reported, see e.g. [90]. We expect that Hubbard models describing trapped imbalanced Fermi gases present a nontrivial scaling behavior as well, sharing most features with the balanced case. In particular, the extension of our analysis to imbalanced fermions in the dilute regime should be straightforward, a universal TSS should be observed, analogously to that found in the balanced case, but with TSS functions also depending on the total spin.

In our paper we mostly focus on 1D systems, but the general features should also apply to higher-dimensional systems, in particular those related to the universal TSS in the dilute regime, the accuracy of the LDA, and the scaling behavior at the boundaries of the trap.

## Appendix A: Mapping between 1D Hubbard and two-flavor Bose-Hubbard models

We discuss the exact mapping between the 1D Hubbard model and the Bose-Hubbard model with two bosonic fields. We consider the two-flavor Bose-Hubbard open chain of length  $L$  with Hamiltonian

$$H_{\text{BH}} = - \sum_{\langle ij \rangle, \alpha} J_{\alpha} (b_{i\alpha}^{\dagger} b_{\alpha j} + b_{\alpha j}^{\dagger} b_{i\alpha}) \quad (\text{A1})$$

$$+ \sum_{\alpha i} U_{\alpha} n_{\alpha i} (n_{\alpha i} - 1) + U_{12} \sum_i n_{1i} n_{2i},$$

where  $b_{i\alpha}$  is a bosonic creation operator and  $\alpha = 1, 2$  and  $n_{i\alpha} \equiv b_{i\alpha}^{\dagger} b_{i\alpha}$  is the particle density. We are interested in the hard-core limit  $U_{\alpha} \rightarrow \infty$ , where  $n_{\alpha i}$  is limited to the values 0 and 1.

Following Ref. 91, we first map the Bose-Hubbard model into a spin-1/2 system through the Holstein-

Primakoff transformation

$$\begin{aligned}\sigma_{\alpha i}^+ &= b_{\alpha i}^\dagger \sqrt{1 - b_{\alpha i}^\dagger b_{\alpha i}}, \\ \sigma_{\alpha i}^- &= \sqrt{1 - b_{\alpha i}^\dagger b_{\alpha i}} b_{\alpha i}, \\ \sigma_{\alpha i}^z &= b_{\alpha i}^\dagger b_{\alpha i} - \frac{1}{2}.\end{aligned}\quad (\text{A2})$$

Then the spin-1/2 system can be mapped into a Hubbard model through the Jordan-Wigner transformation [92]

$$\sigma_{\alpha i}^+ = c_{\alpha i}^\dagger R_{\alpha i}, \quad \sigma_{\alpha i}^- = R_{\alpha i} c_{\alpha i}, \quad \sigma_{\alpha i}^z = c_{\alpha i}^\dagger c_{\alpha i} - \frac{1}{2}, \quad (\text{A3})$$

where

$$\begin{aligned}R_{1i} &= (-1)^{\sum_{j<i} n_{1j}}, \quad R_{2i} = (-1)^{N_1 + \sum_{j<i} n_{2j}}, \\ N_\alpha &= \sum_i n_{\alpha i}.\end{aligned}\quad (\text{A4})$$

The resulting Hamiltonian is exactly the Hubbard model Hamiltonian (1). The above mapping also applies if additional interactions only involving  $n_{\alpha i}$  are present, e.g., a trapping potential as in Eq. (4) or a nearest-neighbor  $nn$  coupling (extended Hubbard model).

Concerning the boundary conditions, while the case of OBC is quite trivial, we note that periodic boundary conditions in  $b$  are not equivalent to periodic boundary conditions in  $c$ .

## Appendix B: The Bethe Ansatz

The Bethe-Ansatz method allows us to solve exactly several 1D models, like the Hubbard model, the XXZ model, the Gaudin–Yang model, etc. This method reduces the complex many-particle scattering process between fermions to the composition of many two-particle processes, where particle momenta are not changed, but merely reassigned to different particles. This physical picture allows us to introduce a wavefunction ansatz where the role of momenta permutations is explicit: the ansatz keeps in account all possible outgoing scattering states, weighted with appropriate amplitudes. Model-specific conditions are used to give conditions about them: in the Hubbard Model [59] this is achieved using boundary conditions, the first quantization Schrödinger equation, and symmetry conditions, obtaining a number of relations called Lieb-Wu equations.

While these equations are in general difficult to solve, in the thermodynamic limit their solutions are approximated by particular solution patterns in the complex plane: assuming that all solutions can be approximated by these patterns allows us to rewrite the Lieb-Wu equations as integral equations which allow us to compute the

thermodynamic quantities of the model. In the absence of external magnetic fields and at  $T = 0$ , the particle density  $\rho(\mu)$  for  $U > 0$  can be determined solving the integral-equation system

$$\begin{aligned}\kappa_Q(k) &= -2 \cos k - \mu + \\ &+ \int_{-Q}^{+Q} dk' R(\sin k' - \sin k) \kappa_Q(k') \cos k', \\ \Pi_Q(k) &= \frac{1}{2\pi} + \cos k \int_{-Q}^{+Q} dk' R(\sin k' - \sin k) \Pi_Q(k'), \\ \rho(Q) &= \int_{-Q}^{+Q} \Pi_Q(k) dk, \\ R(x) &\equiv \int_{-\infty}^{+\infty} \frac{e^{i\omega x}}{1 + e^{U|\omega|/2}} \frac{d\omega}{2\pi},\end{aligned}\quad (\text{B1})$$

where  $|k| < Q$ ,  $\kappa_Q(k)$  is the dressed energy of the relevant elementary excitations of the model over the ground state and  $\Pi_Q(k)$  is the density of particles in the momentum space. The equation  $\kappa_Q(k = \pm Q) = 0$  can be decomposed in further integral equations, which allow us to link the free parameter  $Q \in [0, \pi]$  to the chemical potential  $\mu$ , obtaining  $\rho(\mu) = \rho[Q(\mu)]$ .

The attractive case ( $U < 0$ ) can be reduced to the repulsive one[59] applying appropriate transformations to the Bethe Ansatz Equations and states: in this case, the integral equations defining the density  $\rho(\mu)$  of the model at  $T = 0$  and in absence of magnetic field become

$$\begin{aligned}\epsilon_\Lambda(\lambda) + \int_{-\Lambda}^{+\Lambda} \frac{|U|}{2\pi[U^2/4 + (\lambda - \nu)^2]} \epsilon_\Lambda(\nu) d\nu &= \\ = 4 \operatorname{Re}[1 - (\lambda + iU/4)^2]^{1/2} + 2\mu, \\ \epsilon_\Lambda(\lambda = \pm\Lambda) &= 0, \\ \sigma_\Lambda(\lambda) + \int_{-\Lambda}^{+\Lambda} \frac{|U|}{2\pi[U^2/4 + (\lambda - \nu)^2]} \sigma_\Lambda(\nu) d\nu &= \\ = \frac{1}{\pi} \operatorname{Re}[1 - (\lambda + iU/4)^2]^{-1/2}, \\ \rho(\Lambda) &= 2 \int_{-\Lambda}^{+\Lambda} \sigma_\Lambda(\lambda) d\lambda,\end{aligned}\quad (\text{B2})$$

where  $|\lambda| < \Lambda$ . In this case  $\epsilon_\Lambda(\lambda)$  is the dressed energy of the model excitations, and is function of the spin rapidity  $\lambda$  (fermionic spin rapidities are, as fermionic momenta, quantum numbers parametrizing the Bethe Ansatz solutions).  $\sigma_\Lambda(\lambda)$  is the particle density in the spin rapidity space. As previously, the relation  $\epsilon_\Lambda(\lambda = \pm\Lambda) = 0$  can be decomposed in further integral equations, which allow us to find a relation between the positive parameter  $\Lambda$  and the chemical potential: this yields the relation  $\rho(\mu) = \rho[\Lambda(\mu)]$ .

- 
- [1] I. Bloch, J. Dalibard, and W. Zwerger, *Rev. Mod. Phys.* **80**, 885 (2008).
- [2] S. Giorgini, L.P. Pitaevskii, and S. Stringari, *Rev. Mod. Phys.* **80**, 1215 (2008).
- [3] T. Esslinger, *Ann. Rev. Cond. Mat. Phys.* **1**, 129 (2010).
- [4] X.-W. Guan, M.T. Batchelor, and C. Lee, *Rev. Mod. Phys.* **85**, 1633 (2013).
- [5] M. Campostrini and E. Vicari, *Phys. Rev. Lett.* **102**, 240601 (2009); (E) **103**, 269901 (2009).
- [6] M. Campostrini and E. Vicari, *Phys. Rev. A* **81**, 023606 (2010).
- [7] K. Schönhammer, O. Gunnarsson, and R.M. Noack, *Phys. Rev. B* **52**, 2504 (1995).
- [8] K. Damle, T. Senthil, S.N. Majumdar, and S. Sachdev, *Europhys. Lett.* **36**, 7 (1996).
- [9] D. A. Butts and D.S. Rokhsar, *Phys. Rev. A* **55**, 4346 (1997).
- [10] F. Gleisberg, W. Wonneberger, U. Schlöder and C. Zimmermann, *Phys. Rev. A* **62**, 063602 (2000).
- [11] V. Dunjko, V. Lorent, and M. Olshanii, *Phys. Rev. Lett.* **86**, 5413 (2001).
- [12] C. Menotti and S. Stringari, *Phys. Rev. A* **66**, 043610 (2002).
- [13] M. Rigol, A. Muramatsu, G.G. Batrouni, and R.T. Scalettar, *Phys. Rev. Lett.* **91**, 130403 (2003).
- [14] A. Recati, P.O. Fedichev, W. Zwerger, and P. Zoller, *Phys. Rev. Lett.* **90**, 020401 (2003).
- [15] S. Wessel, F. Alet, M. Troyer, and G.G. Batrouni, *Phys. Rev. A* **70**, 053615 (2004).
- [16] G.E. Astrakharchik, D. Blume, S. Giorgini, and L.P. Pitaevskii, *Phys. Rev. Lett.* **93**, 050402 (2004).
- [17] R.J. Magyar and K. Burke, *Phys. Rev. A* **70**, 032508 (2004).
- [18] S. Fölling, A. Widera, T. Müller, F. Gerbier, and I. Bloch, *Phys. Rev. Lett.* **97**, 060403 (2006).
- [19] G. Xianlong, M. Polini, R. Asgari, and M.P. Tosi, *Phys. Rev. A* **73**, 033609 (2006).
- [20] G. Xianlong, M. Polini, M.P. Tosi, V.L. Campo, K. Capelle, and M. Rigol, *Phys. Rev. B* **73**, 165120 (2006).
- [21] H. Hu, X.-J. Liu, and P.D. Drummond, *Phys. Rev. Lett.* **98**, 070403 (2007).
- [22] G. Orso, *Phys. Rev. Lett.* **98**, 070402 (2007).
- [23] V.L. Campo, K. Capelle, J. Quintanilla, and C. Hooley, *Phys. Rev. Lett.* **99**, 240403 (2007).
- [24] A.E. Feiguin and F. Heidrich-Meisner, *Phys. Rev. B* **76**, 220508(R) (2007).
- [25] M. Casula, D.M. Ceperley, and E.J. Mueller, *Phys. Rev. A* **78**, 033607 (2008).
- [26] X. Gao and R. Asgari, *Phys. Rev. A* **77**, 033604 (2008).
- [27] P. Kakashvili and C.J. Bolech, *Phys. Rev. A* **79**, 041603 (2009).
- [28] N. Gemelke, X. Zhang, C.-L. Hung, and C. Chin, *Nature* **460**, 995 (2009).
- [29] E. Taylor, *Phys. Rev. A* **80**, 023612 (2009).
- [30] Q. Zhou, Y. Kato, N. Kawashima, and N. Trivedi, *Phys. Rev. Lett.* **103**, 085701 (2009).
- [31] M. Rigol, G.G. Batrouni, V.G. Rousseau, and R.T. Scalettar, *Phys. Rev. A* **79**, 053605 (2009).
- [32] S. Trotzky, L. Pollet, F. Gerbier, U. Schnorrberger, I. Bloch, N.V. Prokofev, B. Svistunov, and M. Troyer, *Nat. Phys.* **6**, 998 (2010).
- [33] Q. Zhou and T-L Ho, *Phys. Rev. Lett.* **105**, 245702 (2010).
- [34] T.-L. Ho and Q. Zhou, *Nat. Phys.* **6**, 131 (2010).
- [35] L. Pollet, N.V. Prokofev, and B.V. Svistunov, *Phys. Rev. Lett.* **104**, 245705 (2010).
- [36] L. Pollet, N.V. Prokofev, and B.V. Svistunov, *Phys. Rev. Lett.* **105**, 199601 (2010).
- [37] S. Nascimbene, N. Nayon, F. Chevy, and C. Salomon, *New J. Phys.* **12**, 103026 (2010).
- [38] Q. Zhou, Y. Kato, N. Kawashima, and N. Trivedi, *Phys. Rev. Lett.* **105**, 199602 (2010).
- [39] M. Campostrini and E. Vicari, *Phys. Rev. A* **81**, 063614 (2010).
- [40] M. Campostrini and E. Vicari, *Phys. Rev. A* **82**, 063636 (2010).
- [41] M. Tezuka and M. Ueda, *New J. Phys.* **12**, 055029 (2010).
- [42] F. Heidrich-Meisner, G. Orso, and A.E. Feiguin, *Phys. Rev. A* **81**, 053602 (2010).
- [43] A. Snyder, I. Tanabe, and T. De Silva, *Phys. Rev. A* **83**, 063632 (2011).
- [44] S. Fang, C.-M. Chung, P.-N. Ma, P. Chen, and D.-W. Wang, *Phys. Rev. A* **83**, 031605(R) (2011).
- [45] X. Zhang, C.-L. Hung, S.-K. Tung, N. Gemelke, and C. Chin, *New J. Phys.* **13**, 045011 (2011).
- [46] F. Crecchi and E. Vicari, *Phys. Rev. A* **83**, 035602 (2011); A. Pelissetto and E. Vicari, *Phys. Rev. E* **87**, 032105 (2013).
- [47] K.R.A. Hazzard and E.J. Mueller, *Phys. Rev. A* **84**, 013604 (2011).
- [48] S.A. Söffing, M. Bortz, and S. Eggert, *Phys. Rev. A* **84**, 021602(R) (2011).
- [49] G. Ceccarelli, C. Torrero, and E. Vicari, *Phys. Rev. A* **85**, 023616 (2012).
- [50] L. Pollet, *Rep. Prog. Phys.* **75**, 094501 (2012).
- [51] G. Ceccarelli and C. Torrero, *Phys. Rev. A* **85**, 053637 (2012).
- [52] Y. Khorramzadeh, Fei Lin, and V.W. Scarola, *Phys. Rev. A* **85**, 043610 (2012).
- [53] J. Carrasquilla and M. Rigol, *Phys. Rev. A* **86**, 043629 (2012).
- [54] G. Ceccarelli, C. Torrero, and E. Vicari, *Phys. Rev. B* **87**, 024513 (2013).
- [55] G. Ceccarelli, J. Nespolo, A. Pelissetto, and E. Vicari, *Phys. Rev. B* **88**, 024517 (2013).
- [56] H. Moritz, T. Stöferle, K. Günter, M. Kohl, and T. Esslinger, *Phys. Rev. Lett.* **94**, 210401 (2005).
- [57] Y.-A. Liao, A.S.C. Rittner, T. Paprotta, W. Li, G.B. Partridge, R.G. Hulet, S.K. Baur, and E.J. Mueller, *Nature* **467**, 567 (2010).
- [58] E.H. Lieb and F.Y. Wu, *Phys. Rev. Lett.* **20**, 1445 (1968).
- [59] F.H.L. Essler, H. Frahm, F. Göhmann, A. Klümper, V.E. Korepin, *The One-Dimensional Hubbard Model* (Cambridge University Press, 2005).
- [60] D.S. Petrov, D.M. Gangardt, and G.V. Shlyapnikov, *J. Phys. IV France* **116**, 3-44 (2004).
- [61] T. Giamarchi, *Quantum physics in one dimension* (Clarendon press, 2003).
- [62] S. Sachdev, *Quantum Phase Transitions*, (Cambridge Univ. Press, second edition, 2011).
- [63] M.E. Fisher, M.N. Barber, and D. Jasnow, *Phys. Rev. A* **8**, 1111 (1973).

- [64] A. Pelissetto and E. Vicari, arXiv:1401.0788.
- [65] E. Vicari, Phys. Rev. A **85**, 062104 (2012).
- [66] V. Eisler, Phys. Rev. Lett. **111**, 080402 (2013).
- [67] U. Schollwöck, Rev. Mod. Phys. **77**, 259 (2005).
- [68] M. Gaudin, Phys. Lett. A **24**, 55 (1967).
- [69] C.N. Yang, Phys. Rev. Lett. **19**, 1312 (1967).
- [70] M. Girardeau, J. Math. Phys. (N.Y.) **1**, 516 (1960); M.D. Girardeau, Phys. Rev. **139**, B500 (1965).
- [71] J.N. Fuchs, A. Recati, and W. Zwerger, Phys. Rev. Lett. **93**, 090408 (2004).
- [72] H.J. Schulz, Phys. Rev. Lett. **64**, 2831 (1990).
- [73] L. Guan, S. Chen, Y. Wang, and Z.-Q. Ma, Phys. Rev. Lett. **102**, 160402 (2009).
- [74] C.A. Regal, M. Greiner, and D.S. Jin, Phys. Rev. Lett. **92**, 040403 (2004).
- [75] M.W. Zwierlein, C.A. Stan, C.H. Schunck, S.M.F. Raupach, A.J. Kerman, and W. Ketterle, Phys. Rev. Lett. **92**, 120403 (2004).
- [76] J. Kinast, S.L. Hemmer, M.E. Gehm, A. Turlapov, and J.E. Thomas, Phys. Rev. Lett. **92**, 150402 (2004).
- [77] C. Chin, M. Bartenstein, A. Altmeyer, S. Riedl, S. Jochim, J. H. Denschlag, and R. Grimm, Science **305**, 1128 (2004).
- [78] T. Bourdel, L. Khaykovich, J. Cubizolles, J. Zhang, F. Chevy, M. Teichmann, L. Tarruell, S.J.J.M.F. Kokkelmans, and C. Salomon, Phys. Rev. Lett. **93**, 050401 (2004).
- [79] G.B. Partridge, K.E. Strecker, R.I. Kamar, M.W. Jack, and R.G. Hulet, Phys. Rev. Lett. **95**, 020404 (2005).
- [80] H. Hu, P.D. Drummond, and X.-J. Liu, Nat. Phys. **3**, 469 (2007).
- [81] F. Kalish and D. Braak, J. Phys. A **35**, 9957 (2002).
- [82] M. Machida, M. Okumura, S. Yamada, T. Deguchi, Y. Ohashi, and H. Matsumoto, Phys. Rev. B **78**, 235117 (2008).
- [83] M. Rizzi, M. Polini, M.A. Cazalilla, M.R. Bakhtiari, M.P. Tosi, and R. Fazio, Phys. Rev. B **77**, 245105 (2008).
- [84] W. Bakr, A. Peng, M.E. Tai, R. Ma, J. Simon, J.I. Gillen, S. Fölling, L. Pollet, and M. Greiner, Science **329**, 547 (2010).
- [85] J.F. Sherson, C. Weitenberg, M. Endres, M. Cheneau, I. Bloch, and S. Kuhr, Nature **467**, 68 (2010).
- [86] C.-L. Hung, X. Zhang, L.-C. Ha, S.-K. Tung, N. Gemelke, and C. Chin, New J. Phys. **13**, 075019 (2011).
- [87] M. Endres, M. Cheneau, T. Fukuhara, C. Weitenberg, P. Schauß, C. Gross, L. Mazza, M.C. Banuls, L. Pollet, I. Bloch, and S. Kuhr, Science **334**, 200 (2011).
- [88] M. Cheneau, P. Barmettler, D. Poletti, M. Endres, P. Schauß, T. Fukuhara, C. Gross, I. Bloch, C. Kollath, and S. Kuhr, Nature **481**, 484 (2012).
- [89] P. Fulde and A. Ferrell, Phys. Rev. **135**, A550 (1964); A. Larkin and Y.N. Ovchinnokov, Zh. Eksp. Teor. Fiz. **47**, 1136 (1964) [Sov. Phys. JETP **20**, 762 (1965)].
- [90] M.W. Zwierlein, *et al*, Science **311**, 492 (2006); M.W. Zwierlein, *et al*, Nature **422**, 54 (2006); Y. Shin, *et al*, Phys. Rev. Lett. **97**, 030401 (2006); Y. Shin, *et al*, Nature **451**, 689 (2008); G.B. Partridge, *et al*, Science **311**, 503 (2006); G.B. Partridge, *et al*, Phys. Rev. Lett. **97**, 190407 (2006).
- [91] K. He and M. Rigol, Phys. Rev. A **83**, 023611 (2011).
- [92] E.H. Lieb, T. Schultz and D. Mattis, Ann. Phys. (NY) **16**, 407 (1961).